Graded bed load transport in sediment supply limited channels under unsteady flow hydrographs

Wang, Le; Cuthbertson, Alan J. S.; Zhang, Shang Hong; Pender, Gareth; Shu, An Ping; Wang, Yong Qiang

Published in:
Journal of Hydrology

DOI:
10.1016/j.jhydrol.2021.126015

Publication date:
2021

Graded Bed Load Sediment Transport in a Net Degrading Channel Under Unsteady Flow Hydrographs

Le Wang[1], Alan J S Cuthbertson[2], An Ping Shu[3], Shang Hong Zhang[4], Gareth Pender[5]

[1] Lecturer, School of Water Resources and Hydropower Engineering, North China Electric Power University, Beijing 102206, China. Email: lewang@ncepu.edu.cn

[2] Senior Lecturer, School of Science and Engineering (Civil Engineering), University of Dundee, Dundee DD1 4HN, UK. Email: a.j.s.cuthbertson@dundee.ac.uk.

[3] Professor, School of Environment, Key Laboratory of Water and Sediment Sciences of MOE, Beijing Normal University, Beijing 100875, China. E-mail: shuap@bnu.edu.cn

[4] Professor, School of Water Resources and Hydropower Engineering, North China Electric Power University, Beijing 102206, China. Email: zhangsh928@126.com

[5] Professor, School of Energy, Geoscience, Infrastructure and Society, Heriot-Watt University, Edinburgh EH14 4AS, UK. Email: g.pender@hw.ac.uk

Corresponding author: Alan Cuthbertson (a.j.s.cuthbertson@dundee.ac.uk)

Research Highlights:

- Intrinsic links between unsteady flow hydrographs, graded sediment transport and bed-surface grain size is representative of regulated river reaches.
- Transported fine, medium and coarse size classes show different temporal lags, hysteresis and proportional representations during rising and falling limbs.
- A combined hydrograph descriptor correlates well with bed load yields and bed surface coarsening under zero sediment supply conditions at the inlet.

Abstract

Regulated river channels with limited or no upstream sediment supply can be subject to net bed degradation during natural flood hydrograph events or managed water releases. Heterogeneity in the bed sediment sizes often present in these channels also means that different size classes may be transported preferentially during different parts of the flow hydrograph. A series of laboratory experiments is conducted to investigate the transport response of a graded sediment bed to a range of well-defined unsteady flow hydrographs with a zero-sediment supply condition imposed at the upstream boundary. The results show varying temporal lag and hysteresis patterns for fractional bed load transport, defined for three size classes (fine, medium and coarse) within the graded bed sediment. The coarse size class tends to respond preferentially during the rising limb and typically exhibits a clockwise hysteresis, whereas the fine size class tends to become more active during the falling limb, typically demonstrating no/mixed or counterclockwise hysteresis. On this basis, predictions of bed load transport rates are shown to be improved by calculating separate reference threshold shear stresses for the initiation and cessation of fractional grain motions during the rising and falling limbs, respectively. Corresponding temporal variations of the median grain size within the transported bed load are shown to vary depending on the hydrograph total water work and unsteadiness, with peak values generally attained during the rising limb and an overall fining of bed load observed during the falling limb. Analysis of the three size classes also indicates that the medium-coarse and fine fractions are transported in larger relative proportions during smaller, more flashy hydrographs (i.e. lower total water work and higher unsteadiness) and larger, flatter hydrographs (i.e. higher total water work and lower unsteadiness), respectively. The resulting coarsening of the sediment bed surface layer (i.e. armouring) during the hydrographs is found to be greatest at the upstream end of the test section and decreases exponentially in the downstream direction. Two empirical models,

based on combined hydrograph and bed sediment descriptors, are also shown to predict reasonably well the overall bed load yields generated under design flow hydrographs through the satisfactory collapse of experimental data from the current study, as well as similar previous datasets for both uniform and graded bed sediments.

Keywords: *graded sediment transport, unsteady flow hydrographs, bed load hysteresis, bed surface coarsening, net-degrading channel, bed load yield model.*

1 Introduction

In natural fluvial systems, bed sediments are typically heterogeneous in size, with graded sediment transport linked intrinsically to prevalent unsteady flow conditions within the channel and the upstream supply of sediments. The occurrence of bulk sediment transport is typically concentrated during flood events [e.g. *Berta and Bianco*, 2010; *Lee and Balachandar*, 2012; *Phillips and Sutherland*, 1990], where large volumes of sediment may be mobilised under high peak flows. Furthermore, within regulated river channels, where the upstream supply of sediments is, for example, controlled by the presence of a dam, the potential increase in extreme flood events (i.e. due to climate change) or managed flow releases (i.e. hydropower) has the potential to both increase net bed degradation and alter surficial bed sediment grading in the downstream channel. It is therefore essential to improve current understanding of the sediment transport and bed surface grading changes initiated in regulated river systems in response to the passage of flood events (or managed water releases). This will aid development of improved management strategies for water and sediment resources and, thus, help in the assessment and potential mitigation of socioeconomic impacts arising from fluvial flooding and erosion.

The impact of limiting upstream sediment supply in a regulated river on sediment grain size in the downstream channel has been found from previous experimental and field studies to result in surficial sediment coarsening (i.e. bed armoring) close to the upstream boundary and downstream fining along the channel [*Luo et al.*, 2012; *Morris and Williams*, 1999; *Paola et al.*, 1992; *Rice*, 1999; *Singer*, 2008; *Simon and Rinaldi*, 2006; *Ta et al.*, 2011]. Many of these studies, however, have two obvious shortcomings: firstly, their focus on spatio-temporal variability in grain size distributions developing under steady flow conditions, rather than under unsteady flow (flood hydrograph) events that are more capable of mobilizing and restructuring the bed surface completely. Secondly, their reliance on

individual and synchronous surveys along the length of channel reach, which are particularly time-consuming in large river reaches and incapable of predicting long-term evolution in the downstream bed surface composition. Spatio-temporal changes in bed surface composition are thus expected to follow closely the observed unsteadiness in graded sediment transport and bed degradation during flood hydrograph flows. As such, it is of considerable practical importance to understand the intrinsic links between graded sediment transport processes and the evolving bed surface composition in a non-uniform, net-degrading channel under a wide range of unsteady hydrograph flow conditions.

The inter-granular interactions between coarser and finer sediment grades in a heterogeneous sediment bed mixture are known to influence strongly the fractional bed-load transport rates within a graded sediment bed [*Hassan and Ribberink*, 2005; *Misri et al.*, 1984; *Patel and Ranga Raju*, 1996; *Samaga and Garde*, 1986]. However, the majority of graded bed load sediment transport studies have to-date been conducted under steady flow conditions with a strong focus on quantifying fractional sediment entrainment thresholds and hiding mechanisms [*Saadi*, 2002]. As such, the influence of graded bed sediment exposure and sheltering effects on temporal changes to fractional bed load transport rates under unsteady hydrograph flows remains poorly understood and, thus, represents a primary motivation for the current study.

Furthermore, bulk and fractional bed load sediment yields measured over the duration of an unsteady flow hydrograph event represent important indices for assessing the overall impact of a flood event on fluvial bed evolution (i.e. aggregation/degradation rates and changes to sediment grading). Previous studies have indicated that the unsteadiness of a hydrograph (representative of the rate of change in flow) and total water work (representative of the total flood water volume passing along the channel) influence the total bed load sediment yields measured over the hydrograph duration. In particular, *Lee et al.* [2004]

highlighted that an increase in the unsteadiness of a hydrograph typically resulted in an overall increase in the transported bed load yield, according to a power law. By contrast, *Bombar et al.* [2011] found that normalized bed load yields decreased exponentially as hydrograph unsteadiness increased, while increasing linearly with the total water work. However, these (and other) studies have been limited in the following aspects: (i) parameters representing hydrograph unsteadiness and total water work were not varied independently and therefore their individual effects on measured total bed load yields could not be determined; and (ii) observed relationships between bed load yield and unsteadiness revealed by *Bombar et al.* [2011] had a relatively low correlation ($R^2 = 0.50$) and contradicted an equivalent relationship by *Lee et al.* [2004]. More recently, *Wang et al*. [2015] conducted a systematic study to assess the independent effect of total water work and unsteadiness on total and fractional bed load transport rates and yields for two graded (unimodal and bimodal) sediment mixtures. They found that higher transport yields were obtained when either hydrograph unsteadiness or total water work were increased. Similarly, a bed load yield model proposed by *Waters and Curran* [2015] attempted to combine the influence of total water work and unsteadiness into one hydrograph descriptor parameter. As this model was only tested against their own data, its wider applicability was questioned in a recent study by *Wang et al.* [2019], who themselves derived a modified hydrograph descriptor to better fit a wide range of both uniform and graded sediment transport yield data. As such, the current experimental study builds on the preliminary findings from *Wang et al.* [2015, 2019] and *Waters and Curran* [2015] to provide an improved model that better correlates sediment transport properties, overall bed load yields and bed grading characteristics with individual and combined hydrograph parameters using data obtained from a new series of flume experiments, as well as data from other recent unsteady flow sediment transport experimental studies.

The paper is structured in the following manner. Following this introductory section, scaling considerations for unsteady hydrograph flows and bed load sediment transport are presented in §2. §3 then outlines the experimental program, including the flume set-up, measurement techniques and the range of flow and sedimentary conditions tested. §4 presents the experimental results, focusing on total and fractional bed load transport rates, yields and grain size distribution and the resulting changes to bed surface composition following the passage of design hydrographs tested. §5 and §6 then provide discussion of the key results and findings and the overall conclusions from the study.

2 Scaling Considerations

2.1 Unsteady flow hydrographs

Flow hydrographs are generally comprised of a quasi-steady base (or antecedent) flow of magnitude Q_b, with a superimposed unsteady flow component that increases to a peak flow Q_p over the rising hydrograph limb of duration ΔT_R before decreasing back towards Q_b over the receding limb of duration ΔT_F. The overall magnitude, unsteadiness and shape of unsteady flow hydrographs have been described by three parameters: (i) the *total water work* W_k; (ii) the *unsteadiness* Γ_{HG}; and (iii) the *hydrograph asymmetry* η, each which have been detailed in previous studies [*Wang et al.*, 2015; 2019]. Here, the definition of each parameter is presented briefly. The total water work W_k was proposed originally by *Yen and Lee* [1995], and adopted subsequently by *Lee et al.* [2004] and *Bombar et al.* [2011], to characterise parametrically the magnitude of the unsteady flow component from the passage of a flood hydrograph over an erodible sediment bed, defined as:

$$W_k = \frac{{u_b^*}^2 V_{ol}}{g {H_b}^3 B} \tag{1}$$

where u_b^* is the bed shear velocity for the base flow condition, V_{ol} is the total water volume under the unsteady flow hydrograph (i.e. excluding the base flow), H_b is the initial base flow depth, B is the channel width and g is the gravitational acceleration. The unsteadiness parameter Γ_{HG} was first introduced by *Graf and Suszka* [1985] and *Suszka* [1987] as a function of the ratio of the difference ΔH in water surface elevation between the peak and base flows (i.e. $\Delta H = H_p - H_b$) and the overall hydrograph duration $\Delta T = \Delta T_R + \Delta T_F$, such that:

$$\Gamma_{\mathrm{HG}} = \frac{1}{u_b^*}\frac{\Delta H}{\Delta T} \tag{2}$$

Finally, simple temporal ratio η of the rising and falling limb durations was also used [*Wang et al.*, 2015; 2019] to characterize the hydrograph shape or asymmetry, defined as follows:

$$\eta = \frac{\Delta T_R}{\Delta T_F} \tag{3}$$

Thus, unsteady flow hydrographs with $\eta = 1$ (i.e. $\Delta T_R = \Delta T_F$) typically represent symmetrical hydrographs, while ratios $\eta > 1$ and $\eta < 1$ clearly represent asymmetrical hydrographs with relatively long rising ($\Delta T_R > \Delta T_F$) and falling ($\Delta T_F > \Delta T_R$) limb durations, respectively.

Waters and Curran (2015) proposed a single, non-dimensional hydrograph descriptor variable χ to account for both hydrograph unsteadiness and total flow work parameters, as well as peak flow depth H_p and channel bed median sediment grain size D_{50}, in an attempt to provide a more robust representation of the influence of a particular unsteady flow event on the measured sediment bed load yields. This χ parameter is defined as follows:

$$\chi = \frac{\Gamma_{HG} W_k H_p}{D_{50}} \tag{4}$$

One of the issues with this combined hydrograph parameter is that it proposes implicitly that the separate influences of W_k and Γ_{HG} on measured bed load yields and other sediment transport quantities are equivalent, which was found not to be the case for the uniform sediment experiments conducted in *Wang et al*. [2019]. Indeed, *Wang et al.* [2019] proposed a modified combined hydrograph parameter χ_m to take account of the fact that W_k had a far more dominant influence on uniform bed load sediment yields than Γ_{HG}, with χ_m taking the form:

$$\chi_m = W_k \Gamma_{HG}^{0.2} \left(\frac{H_p}{D_{50}}\right)^{2.5} \tag{5}$$

Sediment yield predictions from Eq. (5) were shown to lie within one order of magnitude of individual data sets over a range of unsteady flows, sediment gradings and upstream boundary conditions. Within the current study, the general applicability of these combined parameters will also be tested on a wider range of experimental data for graded sediment transport under design unsteady hydrograph flows.

2.2 Scaling considerations for bed-load sediment transport

Bed load sediment transport rates are commonly described by the normalized Einstein bed load parameter [*Einstein*, 1942], having the bulk and fractional transport forms:

$$q_b^* = \frac{q_b}{\rho_s \sqrt{\left(\frac{\rho_s}{\rho} - 1\right) g d_{50}^3}} \text{ and } q_{bi}^* = \frac{q_{bi}}{\rho_s \sqrt{\left(\frac{\rho_s}{\rho} - 1\right) g d_i^3}} \tag{6}$$

where q_b and q_{bi} are the total and fractional bed load sediment transport rates (kg m^{-1} s^{-1}), ρ_s and ρ are the sediment and fluid densities, and d_{50} and d_i are the median and fractional sediment grain sizes, respectively. Similarly, the total and fractional sediment mass flux transported over the duration of the unsteady flow hydrograph can also be represented by

normalized total and fractional bed load yield parameters W_t^* and W_{ti}^*, respectively [e.g. *Bombar et al.*, 2011], such that

$$W_t^* = \frac{W_t}{\rho_s b D_{50}^2} \text{ and } W_{ti}^* = \frac{W_{ti}}{\rho_s b D_i^2} \quad (7)$$

where W_t and W_{ti} are the total and fractional bed load mass transport (kg) collected in a sediment trap over the hydrograph duration and b is the sediment trap width (= 0.37 m, i.e. < channel width B). These transport yield parameters W_t^* and W_{ti}^* therefore provide information on the cumulative transport response of the graded sediment bed over the full hydrograph duration, while the individual influence of hydrograph parameters (i.e. Γ_{HG}, W_k, η) and/or their combined effect (i.e. χ or χ_m) on the separate bed load yields attained during the rising and falling hydrograph limbs can be defined by total and fractional bed load yield ratios, ψ_t and ψ_{ti}, as follows:

$$\psi_t = \frac{W_{t,r}^*}{W_{t,f}^*} \text{ and } \psi_{ti} = \frac{W_{ti,r}^*}{W_{ti,f}^*} \quad (8)$$

where subscripts r and f refer to the non-dimensional bed load sediment transport yields measured during the rising and falling hydrograph limbs, respectively. Additional scaling considerations on the dynamic similitude between the laboratory flume studies conducted herein and equivalent conditions expected in natural river channels are considered in the supplementary information (§S3) provided with this paper.

3 Experimental Program

3.1 Flume set-up and bed sediments

The experimental studies were performed in a 22 m-long, 0.75 m-wide and 0.5 m-deep flow-recirculating, tilting flume channel (see Fig. 1). Variable flow rates in the channel were

controlled by a pump frequency inverter capable of producing repeatable, smooth hydrographs (i.e. flow rates varying continually with time) of any desired shape, and with peak flow rates up to 100 l s^{-1} (see Fig. S1 in supplementary information). These unsteady flow conditions were measured using a non-intrusive ultrasonic flow meter in the water supply pipe to the upstream channel inlet. The uncertainty associated with pump performance and flow measurement accuracy (± 0.01 l s^{-1} typically) resulted in minor differences between the flow delivery to the channel and prescribed design flows (see §3.3) and the actual measured flows generated. (Note: statistical analysis indicated an average discrepancy of 0.002 l s^{-1}, while the maximum variability due to instantaneous flow fluctuations was estimated to be ± 0.28 l s^{-1}).

A fine-grained, graded sediment mixture was designed for experimental study from pilot studies on the mobilization of individual sediment fractions under steady flow conditions. The grain size distribution and composition characteristics for this design mixture are detailed in Fig. 2. In order to analyse graded sediment transport behaviour in a more systematic manner, the current study utilized a size classification system proposed by *Kuhnle and Southard* [1988] and *Frey et al.* [2003], whereby the experimental grain size distribution is split into three distinct size classes, termed *fine*, *medium* and *coarse*. The main advantages of this classification is that it: (i) aids description and temporal analysis of the bed load transport composition generated under the unsteady flow hydrographs; (ii) classifies transport behaviour over wider size ranges, thus avoiding stochastic transport properties that may be identified in individual sieved fractions; (iii) reveals possible inter-granular effects, such as exposure of coarser grains and sheltering of finer particles in graded sediment beds [*Ockelford and Haynes*, 2013]; and (iv) enables measurements of fine, medium or coarse bed load rates and yields when some equivalent sieved bed load fractions may be too small to be recorded. As such, fractional expressions for normalised bed load rates, yields and yield

ratios in Eqs. (6) – (8) can equally be applied to these wider size ranges. For the specific design sediment mixture tested in this study, the fine sediment class was defined as d_i = 1.0 – 2.8 mm (d_{50i} = 1.95 mm), the medium grain size class as d_i = 2.8 – 6.3 mm (d_{50i} = 4.0 mm) and the coarse size class as d_i > 6.3 mm (d_{50i} = 9.0 mm), with their relative proportions (by sieved weight) in the graded sediment mixture (Fig. 2) of ~44%, ~38% and ~18%, respectively. No additional sediments were supplied at the upstream end of the flume channel during each experimental run and, as such, simulate zero-sediment feed conditions often associated with regulated river reaches (e.g. downstream of a dam).

3.2 Experimental procedure

Prior to each experimental run, the graded sediment bed was scraped flat using the screed board to produce a bed layer of uniform thickness ~11 cm along the 13.5 m test section of flume channel. The upstream 5 m and downstream 3 m of the flume bed were artificially roughened with open-work gravel (d_{50} = 40 mm and 20 mm, respectively) to (i) ensure a fully developed turbulent boundary layer was established prior to the start of the test section, and (ii) prevent the transport of sediments beyond the end of the channel (see Fig. 1).

All experimental runs were conducted with an initial longitudinal bed slope S_0 of 0.002 and a constant base (antecedent) flow rate of Q_b = 17.0 l s^{-1} and depth H_b = 0.059 m. The initial procedure to set-up steady, uniform base flow conditions along the flume channel prior to the onset of the unsteady hydrograph flow is detailed in the supplementary information (§S1).This initial base flow was designed to satisfy near-threshold of motion conditions for the graded sediment bed, based on the estimated critical Shields stress parameter $\tau_{b,cr}^*$ for the fine size class in the design sediment mixture (see §S1 for details). The base flow condition was maintained for a relatively short period of 15 minutes to rework and stabilize the sediment bed layer prior to the onset of the design flow hydrographs.

Temporal variations in the inflow rates and water surface elevations were measured synchronously over the duration of the unsteady flow hydrograph by the ultrasonic flow meter in the water supply pipe and ultrasonic level sensors located at the inlet and outlet of the channel, respectively (see Fig. 1). Bed load sediment transport rates were measured directly from samples collected in a sediment trap located towards the downstream end of the test bed section. The sampling time intervals varied between 5 and 60 minutes for different runs according to the sediment transport intensity and overall hydrograph duration (see Table 1). After the completion of each run and the sediment bed in the flume was fully drained, samples of the bed surface sediments were collected carefully at 2 m intervals along the test channel and analysed through sieving to determine the longitudinal changes in surface sediment grading.

3.3 Design flow hydrographs

Four groups of design flow hydrographs were tested (see Table 1 and Fig. S1 in supplementary information) within which either the hydrograph asymmetry η (group S1), total water work W_k (group V1) or unsteadiness Γ_{HG} (group U1) were varied systematically with respect to benchmark hydrographs (highlighted runs in Table 1). Within each experimental grouping, the individual influence on bed load sediment transport and bed surface grading from the hydrograph parameter under consideration was tested while other parameters were held largely constant. This was achieved by adjusting peak flows Q_p and hydrograph durations ΔT between different runs to vary W_k and Γ_{HG} (Groups V1 and U1, respectively, Table 1 and Fig. S1), and the relative durations of the rising ΔT_R and receding ΔT_F hydrograph limbs to vary η for fixed Q_p and ΔT values (Group S1, Table 1 and Fig. S1). The majority of design hydrographs tested were symmetrical (i.e. $\eta = 1$). This was deemed the most appropriate shape to determine systematically the effects of W_k and Γ_{HG} on

measured sediment transport rates, hysteresis patterns and bed load yields, as the rate of change of flow rate *dQ/dt* was, by definition, symmetrical during the rising and receding hydrograph limbs. An additional group (UV) of three symmetrical hydrographs was tested with the same peak flow Q_p (= 58.0 l s^{-1}) and progressively shorter durations (i.e. ΔT = 14,400 $\rightarrow$ 7,200 $\rightarrow$ 3,600 s), leading to a reduction in W_k and increase in Γ_{HG} values (see Table 1). This latter group was used specifically to test the development and application of combined hydrograph parameters for the estimation of overall bed load sediment yields (see §4.1.3). [Note: full details of all dimensional total and fractional bed load transport yields generated during the overall design flow hydrographs, and separately during the rising and falling limbs, are given in Table S1 of supplementary information.]

4 Results

4.1 Non-uniform bed load sediment transport properties

Bed load sediment transport properties including peak transport rate $q_{b,max}$, bulk sediment yield W_t and yield ratio ψ_t, and transport hysteresis patterns are summarized in Table 2 for all design hydrograph flow conditions tested.

4.1.1 Bed load sediment transport rates

Example plots of both bulk and size-class separated bed load transport rates (q_b and q_{bi}, respectively) generated over different design hydrographs are presented in Fig. 3. All equivalent plots from hydrograph groups S1, U1 and V1 (Table 1) showing the individual effects of η, Γ_{HG} and W_k, respectively, are provided in supplementary information (Fig. S2). For the bulk bed load transport rates, it is apparent from these plots that q_b values generally increase during the rising hydrograph limb and decrease during the receding limb, as expected, with peak transport rates $q_{b,max}$ occurring around the peak flow value Q_p. The

overall magnitude of $q_{b,max}$ is shown to be largely unaffected by hydrograph shape [i.e. varying η, Figs. 3(a) and (b), Table 1], while it decreases systematically with reducing values of Γ_{HG} [i.e. Fig. 3(c), Table 1] and W_k [i.e. Fig. 3(d), Table 1]. The results present no conclusive evidence of a consistent positive or negative temporal lag between Q_p and $q_{b,max}$, due partly to the variable bed load sampling time interval for different design hydrographs (see Table 1). However, many of the measured q_b values around the peak flow regions do show a positive temporal lag (i.e. peak bed load transport occurring after peak flow), indicative of (i) the inertial response of bed load sediment transport to the time-varying flow conditions, and/or (ii) differential transport rates for different size classes during the rising and falling hydrograph limbs.

The temporal variations in measured q_{bi} values for the individual fine, medium, coarse sediment size classes are also presented in Fig. 3 (and, again, in Fig. S2 for all runs in groups S1, U1 and V1 – see supplementary information). The bed load transport rates for the coarse size class are shown to be significantly lower than for the medium and fine size classes, partly due to the overall grading of the design sediment mixture (see Fig. 2) and partly to the reduced mobility of larger grains within the sediment mixture. Within these fractional bed load transport results, it is observed that the coarse (and, on occasion, medium) size classes can attain their peak transport rates $q_{bi,max}$ at an earlier elapsed time than the fine size class. Indeed, within most runs, $q_{bi,max}$ for the coarse size class occurs during the rising limb (i.e. before peak flow), while $q_{bi,max}$ for the fine size class is typically attained during the falling limb (i.e. after peak flow). A similar size-dependent temporal lag in peak bed load transport rates for fine, medium and coarse size classes defined for unimodal and bimodal sediment mixtures tested under unsteady flow hydrographs was reported in smaller scale flume studies conducted by *Wang et al.* [2015].

4.1.2 Bed load hysteresis

Direct phase plots of total q_b and fractional q_{bi} bed load transport rates versus flow rate Q are used to classify the bed load transport hysteresis for the range of hydrographs tested. Example phase plots are presented in Fig. 4 for the same runs as presented in Fig. 3 for bulk and size-class separated bed load transport [note: all phase plots are provided in Fig. S3 of supplementary information]. For the η-varying hydrographs (group S1), both bulk and size-class separated bed load transport rates are generally shown to display *clockwise* (CW) hysteresis (i.e. larger q_b values obtained on the rising limb than on the receding limb at equivalent flow rates) over the majority of the hydrograph duration. The exception to this is around the peak flow region, where differences in q_b values at equivalent flow rates on the rising and receding limbs diminish. This finding is consistent with previous studies of *Humphries et al.* [2012] and *Mao* [2012].

The differences in bulk and size-class separated bed load transport rates between the rising and falling limbs (and, hence, transport hysteresis patterns) are shown to change as Γ_{HG} reduces. For bulk bed load transport, variation in observed hysteresis is from *no/mixed* (N/M) to *counterclockwise* (CCW) hysteresis for design hydrographs U1a $\rightarrow$ U1e (see Table 2, Fig. S3). By contrast, the coarse size class is observed to have general CW hysteresis for all Γ_{HG} values (except for the N/M hysteresis observed in run U1e with the lowest Γ_{HG} value, Table 2). Correspondingly, the fine size class varies from N/M hysteresis at larger Γ_{HG} values to CCW hysteresis at lower Γ_{HG} values, with the medium size class following either these coarse or fine hysteresis patterns. Overall, this indicates that an increasing proportion of the total and size-class separated bed load yields are transported during the receding limb as the hydrograph unsteadiness reduces. A similar, but less consistent, influence from W_k on bulk transport hysteresis is also observed, with an overall trend of N/M $\rightarrow$ CCW hysteresis with a reduction in W_k. Again, the coarse size class demonstrates a transition from CW to N/M

hysteresis between runs V1a to V1e (Fig. S3, Table 2), while the fine size class varies between N/M and CCW hysteresis patterns over the same runs. In general, the hysteresis patterns for the bulk bed load transport tend to follow the fine and/or medium size class hysteresis patterns (as opposed to the coarse size class), as these represent the dominant constituents of the design sediment mixture (see Fig. 2). Furthermore, the observed variations in hysteresis patterns between the coarse and fine size classes suggest that coarse grain sizes are transported "preferentially" at earlier stages in the hydrographs (i.e. during the rising limb), while fine grain sizes are transported "preferentially" at later stages in the hydrographs (i.e. during the receding limb). Similar size-dependent lag effects and hysteresis patterns were observed in previous experimental studies by *Wang et al.* [2015] and *Guney et al.* [2013] testing bimodal sediment mixtures under unsteady hydrograph flows.

4.1.3 Bed load sediment yields

The individual influences of hydrograph parameters η, Γ_{HG} and W_k on the normalized total and size-class separated bed load yields, W_t^* and W_{ti}^* (Eq. 7), as well as the equivalent yield ratios ψ_t and ψ_{ti} (Eq. 8) between the rising and receding limbs are analysed in this section.

As shape parameter η was already found to have a negligible effect on overall bed load yields [*Wang et al.*, 2015; 2019], here, we focus on impacts of total water work W_k and unsteadiness Γ_{HG} on bulk and fractional bed-load yields resulting from the mobilisation of graded bed sediment under unsteady flow hydrographs. The individual parametric relationships between parameters Γ_{HG} and W_k and the non-dimensional total and fractional bed-load yields W_t^* and W_{ti}^* are shown in Fig. 5. It is apparent in Figs. 5(a) and (b) that both W_t^* and W_{ti}^* values increase significantly with increasing values of total water work W_k and Γ_{HG} (i.e. for fixed Γ_{HG} and W_k values, respectively – groups S1, V1 and U1, Table 1). Both the total and fractional bed load yields demonstrate comparable high levels of correlation (R^2 >

0.95) with similar best-fit power law relationships of the general form: $W_t^* = c_1 W_k^m$ and $W_t^* = c_2 \Gamma_{HG}^n$, where c_1, c_2, m and n are empirical coefficients. It is interesting to note that the power exponents of the best fit regression lines for the total, fine and medium sediment size fractional yields are approximately equal [i.e. m = 2.39 – 2.57, n = 1.60 – 1.64, Fig. 5(a) and (b)], while the coarse size fraction yield has larger exponent values [i.e. m = 2.76, n = 2.49].

Indeed, the fact that the power exponents $m > n$ also suggests that total water work W_k has a greater overall influence on the magnitude of bed load yields than unsteadiness Γ_{HG}. A combined hydrograph parameter ξ_g that accounts for the relative influence of W_k and Γ_{HG} can thus be developed in a similar manner to *Wang et al.* [2019], where the most appropriate form of this combined parameter is $\xi_g = W_k \Gamma_{HG}^{\alpha}$, within an adjusted general power law relationship: $W_t^* = c_3 \xi_g^{\beta}$. Further regression analysis of the total and fractional sediment transport yields determines that exponent α = 0.63 provides the best overall correlation (R^2 > 0.91) to the bulk W_t^* and fractional W_{ti}^* values [Fig. 5(c)] (with β = 2.49 – 3.02). This is clearly different from $\xi_g = W_k \Gamma_{HG}^{0.2}$ (i.e. α = 0.2) obtained for the bulk transport of quasi-uniform-sized sediments in *Wang et al.* [2019]. This difference is attributed to bed sediment grading and the fact that lower intensity bed load transport rates measured from the graded sediment bed are more sensitive to the changing flow hydrograph characteristics than the larger magnitude bed load transport rates generated from quasi-uniform bed sediments under equivalent flow hydrograph conditions. This finding is intrinsically consistent with previous studies [e.g. Wilcock and Crowe, 2003; Recking et al., 2009], where the rate of change in bed load sediment transport (i.e. dq_b/dt) is greater when the bed load rate q_b is lower. This implies that hydrograph unsteadiness Γ_{HG} will tend to have a stronger control on bed load yields when the magnitude of bed load yield is lower. This finding is also supported when comparing the relative influence of W_k and Γ_{HG} on fractional bed load yields W_{ti}^* [Figs. 5(a)

and (b)]. Here, the impact of Γ_{HG} on the bed load yields of the coarse fraction is shown to be comparable to that from W_k (i.e. exponent $m \approx n$), whereas the relative influence of Γ_{HG} on bed load yields for the bulk, medium and fine fractions is significantly reduced compared to W_k (i.e. $m > n$), as discussed previously.

4.2 Bed load and bed surface composition

In addition to the analysis of total and fractional bed load transport rates and yields, it is informative to consider how the median size of the bed load sediment transport d_{b50} varies throughout the design flow hydrographs and how the bed surface d_{s50} is changed by the passage of the hydrograph with respect to the initial bed condition.

4.2.1 Bed load composition

It is shown that the median grain size d_{b50} of the bed load sediment transport in η-varied hydrographs [S1a – S1c, Figs. 6(a)-(c)] are generally found to occur during the rising limb or around peak flow, corresponding to the preferential transport of the coarse size class during this period (as noted previously). Overall, analysis of the collected bed load samples indicates some degree of coarsening during the rising limb and fining during the falling limb. It is particularly interesting to note that in all cases, the median size of the transported material is significantly lower than the median grain size of the initial bed sediment grading (i.e. $d_{b50} <$ 2.4 mm) throughout the duration of the hydrographs.

Similar example plots of the temporal variation in d_{b50} for design hydrographs with varying unsteadiness Γ_{HG} are shown in Figs. 6(d)-(g). Here, a general trend is observed that d_{b50} decreases relatively consistently during these hydrographs, which is especially notable under hydrographs with lower unsteadiness Γ_{HG} (i.e. hydrographs with the longest overall durations and the lowest peak flows in this study). This bed load fining trend differs from

both the uni and bimodal bed load transport found in *Wang et al.* [2015], most probably due to a combination of effects, including a more appreciable impact from the no upstream sediment supply configuration on bed degradation and surface coarsening under the range of design flow hydrographs tested in the current study. This, in turn, influences the composition of the transported bed load sediment composition, and is in general agreement with findings from *Hassan et al.* [2006]. Other factors may include non-equal sediment transport mobility [*Wilcock and McArdell*, 1993], where from the overall reduction in flow magnitude within hydrographs U1a $\rightarrow$ U1e, it can be inferred that particles in the coarser size class became more difficult to mobilize (see Figs. 3 and 4, and transport rates and yields in Table 2). By contrast, the relatively high availability and mobility of the fine and medium size classes within the graded sediment mixture, especially under flow hydrographs where the mobility of the coarser size class is reduced, indicates that the peak bed load d_{b50} will occur during the rising limb and then reduce consistently throughout the hydrograph.

Figs. 6(h)-(k) provide similar information on the temporal variation in d_{b50} under design hydrograph conditions with varying W_k. Here, the representative bed load d_{b50} demonstrates a general increase on the rising limb and decrease on the falling limb (i.e. for tests V1a $\rightarrow$ V1d), as shown previously in the η-varying hydrographs [Figs. 6(a)-(c)]. However, it is also shown in run V1e that d_{b50} only varies slightly and remains approximately at the same level. The variations in d_{b50} within hydrographs V1b $\rightarrow$ V1e are controlled largely by the shorter hydrograph durations and the larger proportion of coarse size class available to be transported on the rising limb when compared to equivalent d_{b50} measurements made in runs U1b $\rightarrow$ U1e (i.e. for reducing Γ_{HG} values). Taking a comprehensive overview of the d_{b50} variations for the runs in experimental groups U1 and V1 (i.e. Table 1), it can be surmised that the bed load transport d_{b50} size shows: (i) relatively little variability in short-duration, low magnitude, hydrographs [i.e. run V1e with low W_k, Fig.

6(e)]; (ii) initial bed load coarsening on the rising limb then fining on the falling limb for hydrographs V1d → V1a with increasing peak flow and duration [i.e. increasing W_k and fixed Γ_{HG}, Figs. 6(a),(h)-(j)]; and (iii) continuous bed load fining for hydrographs U1b → U1e with increasing duration and reducing peak flow [i.e. reducing Γ_{HG} and fixed W_k, Figs. 6(d)-(g)].

4.2.2 Post-hydrograph bed surface composition

The change in the bed surface composition from the initial bed sediment mixture grading was measured following the passage of the individual design flow hydrographs through manual sampling along the test sediment bed (see §3.2). Fig. 7(a) presents the spatial variation in bed surface composition d_{s50} under the η-varied hydrographs (i.e. S1a-S1c, Table 1). It is clear that the d_{s50} values are significantly coarser at upstream end of the test section, then reduce asymptotically with increasing distance along the test sediment bed, although remaining above the initial median size d_{50} of the graded bed sediment mixture (i.e. $d_{s50} > 2.64$ mm, Fig. 2). It is also noted that the d_{s50} values at the upstream end of the test bed section were largest after the passage of the flow hydrograph with the shortest duration rising limb (i.e. $\eta = 0.4$) and reduced systematically as η increased (i.e. as the duration of the rising limb increased). Similarly, Figs. 7(b) and (c) present the equivalent spatial variations in d_{s50} values following the passage of flow hydrographs with varying Γ_{HG} and W_k values, respectively. These plots also imply that a coarser bed surface is generated at upstream end of the test bed, especially following design hydrographs with higher unsteadiness Γ_{HG} and larger total water work W_k. By contrast, the remaining length of the test bed surface (i.e. $x = 4.0$ m → 12.0 m, Fig. 7) is relatively less sensitive to variations in the hydrograph parameters η, Γ_{HG} and W_k, but remains consistently above $d_{s50\text{-}ini} = 2.40$ mm. This also indicates that the initial sediment placement along the test section of the flume channel (Fig. 1) and/or the sub-threshold, antecedent flow conditions may have contributed to a general initial coarsening of the bed

surface layer. The exact mechanisms for any initial bed surface coarsening will depend on sediment bed grading and, specifically, the ability of finer fractions at the surface to migrate progressively into deeper substrate pore space within the gravel mixture [e.g. *Wilcock et al.*, 2001; *Wilcock and Crowe*, 2003], resulting in the formation of a coarsened or static armoured surface layer [e.g. *Wilcock and DeTemple*, 2005; *Parker et al.*, 2007] occurring under the antecedent-flow phase of the experimental runs [*Piedra*, 2010].

Finally, Fig. 7(d) presents the relationship between the non-dimensional, coarsened surface median grain size d_{s0}^* (= $d_{s50}/d_{s50\text{-}ini}$) at the upstream end of the bed test section (i.e. x = 0 m) and the combined hydrograph parameter ξ_g (= $W_k\Gamma_{HG}^{0.63}$). This shows clearly that the relative bed surface coarsening d_{s0}^*, immediately downstream of the zero-sediment feed condition imposed at the channel inlet, increases as ξ_g increases (i.e. either through an increased hydrograph unsteadiness Γ_{HG} or total water work W_k). As anticipated by the well-defined power-law relationships between total W_t^* and fractional W_{ti}^* bed load yields and ξ_g, discussed above, d_{s0}^* is also shown to correlate well with ξ_g, following a similar best-fit power law relationship:

$$d_{s0}^* = 1.89\xi_g^{0.214} \qquad (R^2 = 0.77) \qquad (9)$$

Our analysis of bed surface coarsening will be extended further to consider the apparent asymptotic adjustment in d_{s50}^* along the normalized length of the test bed section x^* = x/L within the subsequent discussions (§5.4).

5 Discussion

5.1 Variability in dimensionless bed load transport rates

The observed temporal variability in bed load sediment transport in response to the unsteady design flow hydrographs and zero-sediment supply conditions imposed at the upstream

boundary is characterized by differential transport rates during the rising and falling limbs. To account for this variability, *Waters and Curran* [2015] proposed an analytical approach whereby the bed load transport is predicted separately on the rising and falling hydrograph limbs. This is obtained through evaluation of a dimensionless transport rate W_i^*, using the Einstein-Parker dimensionless reference shear stress approach [*Parker et al*., 1982], which can be written for transported fine, medium and coarse size classes in the form:

$$W_i^* = m\left(1 - 0.8531\frac{\tau_{bir}^*}{\tau_{bi}^*}\right)^n \quad (10)$$

where τ_{bir}^* corresponds to a dimensionless reference transport rate for the fine, medium and coarse size classes (denoted by subscript *i*) of $W_i^* = q_{bi}^*/{\tau_{bi}^*}^{3/2} = 0.002$, and *m*, *n* are modified transport coefficients derived using nonlinear regression [*Waters and Curran*, 2015], with their original values *m* = 11.2 and *n* = 4.5 according to *Parker et al.* [1982]. Eq. (10) can therefore be fitted to all bed-load transport data measured over the different design flow hydrographs tested in this study, as well as the limb-separated datasets (i.e. transport rates on rising and receding limbs). According to the reference sediment transport rate $W_i^* = 0.002$, the reference dimensionless shear stress τ_{bir}^* were determined from the overall, rising and falling limb bed load transport data for the fine (i.e. τ_{bir}^*= 0.0342, 0.0336 and 0.0347), medium (i.e. τ_{bir}^* = 0.0179, 0.0171 and 0.0187) and coarse (τ_{bir}^*= 0.0100, 0.0093 and 0.0106) fractions. It is apparent that the reference shear stresses for bed load transported by rising flow are consistently lower than for sediment transport during the falling limb, whereas the overall shear stresses across the whole hydrograph are found to lie in between the rising and falling limb values, regardless of the sediment size class.

The overall bed load data show a good general agreement with Eq. (10) predictions of the bed load transport curve for derived coefficient values *m* = 11.2 and *n* = 4.5 (i.e. solid black line, Fig. 8). Best-fit regression trend lines to the data (i.e. dashed lines, Fig. 8) also

indicate good agreement with Eq. (10) at lower dimensionless transport rates (i.e. W_i^* >1) but deviate from the Einstein-Parker relationship at higher W_i^* values. This appears to be associated with lower reference stress τ_{bir}^* derived for the three size classes transported under the current design flow hydrographs that are characterized by continuously varying flow rates with time (i.e. *dQ/dt*). For example, *Waters and Curran* [2015] obtained τ_{bir}^*= 0.079 for the sand fraction within a sand-gravel mixture under stepped hydrograph flows, while τ_{bir}^*= 0.0342 was obtained for sand fraction in our study. This implies that the bed sediments are more susceptible to mobilization under smooth, unsteady flow hydrographs than under stepped flow hydrograph flows that are basically composed with an incrementally changing series of steady flows. Figs. 8(b) and (c) also shows the best fit using the separate-limb method, outlined by *Waters and Curran* [2015], with regression of the falling limb data having the highest R^2 (= 0.81) value, followed by the rising limb (R^2 = 0.74) and then the overall (R^2 = 0.72) bed load transport rate data. This limb-dependent approach therefore provides better fit to observed bed load rate data than considering the overall transport data set throughout the whole duration of the design hydrographs. From a process-based perspective, the separate-limb method is also shown to account better for the differential effects of the rising and falling limbs on sediment transport compared with methods that consider the sediment transport characteristics over the full duration of the flow hydrograph. This is due to the apparent differential bed load transport behavior of the fine, medium, and coarse size classes mobilized under the same flow conditions on rising and falling limbs, resulting in differential hysteresis in the fractional bed load transport rates (see §5.2). This suggests that the positive or negative flow gradient (*dQ/dt*) could contribute to the initiation or termination of the fractional sediment motion during the rising and falling limbs. This seems reasonable as the sediment bed surface is initially activated in response to increasing flow (i.e. *dQ/dt* > 0), while the mobile sediment bed becomes inactive again due to reducing

flow (i.e. $dQ/dt < 0$) with an armored surface layer having developed (Fig. 7). This is also supported by the fact that the lowest W_i^* values are achieved specifically for coarse and medium size classes during the falling limb of the design hydrographs [shown in Fig. 8(b) and (c)].

5.2 Variability in bed load hysteresis

It is well-recognized that five common classes of hysteresis are reported for bed load sediment transport under unsteady flow hydrograph, defined as: (i) *single-valued*, (ii) *clockwise*, (iii) *counter-clockwise*, (iv) *single-valued plus a loop*, and (v) *figure-8* [e.g. *Waters and Curran*, 2015; *Williams*, 1989]. In our study, the hysteresis patterns for the graded sediment transport under all design hydrographs tested were grouped into the three general classifications of *clockwise* (CW) [i.e. (ii)], *counter-clockwise* (CCW) [i.e. (iii)], and *no/mixed hysteresis* (N/M) [i.e. (i), (iv) and (v)] (see Fig. 4 and S3), which are the same definitions for hysteresis as considered in the recent study of quasi-uniform sediment transport under unsteady design flow hydrographs [*Wang et al.*, 2019]. Within this previous study, it was also found that the bed load transport hysteresis showed a good correlation with the ratio of bed load yields ψ_t obtained during rising and falling limbs of the symmetrical design flow hydrographs. This association is extended by calculating equivalent fractional yield ratios ψ_{ti} for the individual size classes transported in the graded bed sediment tests considered herein. Specifically, the different bed load transport hysteresis for the coarse, medium and fine size classes, along with the bulk sediment transport, are plotted for all symmetrical design hydrographs in the W_k: Γ_{HG} space domain in Fig. 9, along with their respective fractional and total bed load yield ratios ψ_{ti} and ψ_t. It is clear that the coarse and medium size classes show a dominance of CW and N/M hysteresis in the bed load transport [Fig. 9(a) and (b)], where CW hysteresis is typically obtained for hydrographs with higher

total water work W_k and/or unsteadiness Γ_{HG}, tending to change to N/M hysteresis as either W_k and/or Γ_{HG} reduce. Accordingly, the majority of fractional bed load ratios ψ_{ti} (and corresponding run-averaged $\bar{\psi}_{ti}$ values) are greater than unity (i.e. with larger bed load yields obtained during the rising limb). By contrast, no CW hysteresis is obtained for the bed load transport of the fine size class, which transitions between N/M and CCW hysteresis again as Γ_{HG} and/or W_k values reduce [Fig. 9(c)]. Here, the majority of ψ_{ti} values are less than unity, indicating larger bed load transport yields were obtained during the falling limb. These grain size dependence of changes to the bed load hysteresis patterns are largely attributed to inter-granular effects. Specifically, coarser particles are generally expected to more exposed on bed surface and, thus, can be mobilised more actively during the rising limb in response to the increasing flow rate (i.e. $dQ/dt > 0$) than the more sheltered finer grains [e.g. *Ockelford and Haynes*, 2013], which are transported preferentially during the falling limb. It is also interesting to note that the bed load hysteresis for the bulk sediment transport [Fig. 9(d)] largely follows the same hysteresis patterns as obtained for the fine size class [Fig. 9(c)]. This clearly demonstrates the relative dominance of the fine size class within the total bulk transport, as previously indicated by the total and fractional bed load yields plotted in Fig. 5. However, most total bed load ratios ψ_t (and the corresponding run-averaged $\bar{\psi}_t$ value) for the bulk sediment transport are close to unity, which results from the relative mobility of different size classes at different points during the hydrograph.

Through careful examination of the correspondence between fractional bed load transport hysteresis and bed load yields ratios ψ_{ti} (as listed in Table 2), it is shown that well-defined CW or CCW hysteresis patterns correspond universally to symmetrical design hydrographs where the resulting bedload yield ratios $\psi_{ti} >> 1.0$ and $\psi_{ti} << 1.0$, respectively. However, it is also shown that all runs with $\psi_{ti} > 1.0$ and $\psi_{ti} < 1.0$ do not necessarily generate

CW and CCW hysteresis patterns, with a number of runs with $\psi_{ti} \approx 1$ generating N/M hysteresis patterns.

5.3 Variability in bed load sediment transport yields

Within managed or regulated river reaches, where the upstream sediment supply is controlled (e.g. by the presence of dam), assessment of bed load sediment yields generated directly from in-channel, stored bed sediments is critical to determining the spatial variability in net erosion and deposition, the development of morphological bed forms, and changes to the surface grain size distribution following hydrograph flow events. In our study, the individual and collective influence of hydrograph parameters η, Γ_{HG} and W_k on total and fractional bed load transport properties is comprehensively studied. It was clear from regression analysis that the total water work W_k has a greater overall influence on the measured bed load yields than the unsteadiness Γ_{HG} [see Fig. 5(a) and (b)], with a combined hydrograph parameter $\xi_g = W_k\Gamma_{HG}^{0.63}$ found to provide best overall fit to the total and fractional bed load yields [Fig. 5(c)]. This compares to $\xi_g = W_k\,\Gamma_{HG}^{0.2}$ obtained in a previous experimental study from regression analysis of bed load yields measured in quasi-uniform bed sediments under a similar range of design flow hydrographs [*Wang et al.*, 2019]. They also demonstrated that the bed load yield W_t^* data obtained from a wide range of previous studies with graded (sand/gravel, sand/silt) and uniform (sand, gravel) sediments collapsed satisfactorily (within one order of magnitude) when plotted against a combined parameter $\chi_m = \xi_g(H_p/d_{50})^{2.5}$ (as defined previously in Eq. 5). Here, we can compare directly the overall level of model fit to total bed load yield W_t^* data from the current and previous studies by using the two versions of ξ_g outlined above [i.e. Figs. 10(a) and (b)]:

$$\chi_{m1} = W_k\Gamma_{HG}^{0.63}\left(\frac{H_p}{d_{50}}\right)^{2.5};\ \ \chi_{m2} = W_k\Gamma_{HG}^{0.2}\left(\frac{H_p}{d_{50}}\right)^{2.5} \tag{11}$$

Overall, the level of data agreement of the two derived power laws in Figs. 10(a) and (b), both with general form $W_t^* = a.\chi_m^{\ b}$, is shown to be similar (R^2 = 0.74 and 0.79, respectively), with both indicating the vast majority of W_t^* data lie within one order of magnitude of the respective power law prediction. It is important to note here that the model performance will only be satisfactory if the threshold flow required to initiate sediment motion during the rising limb of the hydrograph is only slightly higher than base flow rate (or antecedent flow). Caution is therefore required when applying the above formulations if these threshold flow conditions are well above the base flow condition. In this case, the bed load yields W_t^* predicted by the power law expressions in Figs. 10(a) and (b) will be significantly over-estimated. It is also clear from these composite W_t^*: χ_m plots that the uniform (sand) bed load transport conditions of *Wang* [2016] and *Lee et al.* [2004] typically lie above the power law relationships, while the graded sand/gravel bed load transport conditions (including the present study) generally lie beneath these relationships. This in due to the increased mobility of the uniform bed sediments (where the flow rate required for incipient motion was just above base flow) compared to the graded bed sediments (requiring higher flow rates for incipient motion) under equivalent W_k and Γ_{HG} varying hydrographs. This is, to an extent, reflected in the relatively low non-dimensional bed load transport rates W_i^* measured around τ_{bi}^*/τ_{bir}^* = 1 shown in Fig. 8 [i.e. $O(10^{-3} – 10^{-2})$] compared to $W^* = O(10^{-2} – 10^{-1})$ at τ_b^*/τ_{br}^* = 1 for the quasi-uniform sand tested in *Wang et al.* [2019] (see Fig. 8). Consequently, a greater variability on the impact of W_k and Γ_{HG} is reflected in the bed load yields measured for the graded sediment transport, with the contribution of Γ_{HG} in particular shown to become more significant than for the quasi-uniform sediment transport.

5.4 Variability in bed load and bed surface composition

Analysis of the bed load sediment samples collected at different stages throughout the different design flow hydrographs tested suggests that the temporal variation in sediment transport composition (represented by median bed load grain size d_{b50}) is influenced by the hydrograph unsteadiness Γ_{HG} and total water work W_k. Overall, there is a general net fining of bed load during the hydrographs, although larger magnitude hydrographs (i.e. high W_k values) and shorter duration events appear also to result in initial coarsening of bed load during the rising limb prior to general fining in the falling limb (Fig. 6). It is also interesting that, for the zero-sediment feed conditions imposed at the upstream inlet, median bed load size d_{b50} is always considerable finer than the initial surface median size of the graded bed sediment $d_{s50\text{-}ini}$ = 2.40 mm, suggesting that the sediment bed and surface layer in particular must, by definition, coarsen. These temporal variations in bed load composition are clearly a direct reflection on the proportions of fine, medium and coarse size classes that are mobilised at any given time throughout the duration of the design hydrographs (i.e. relative fractional transport rates $q_{bi,}$ Fig. 3). In this respect, the relative mobilisation of the different size classes during the rising and falling limbs, in comparison to over the full design hydrograph is reflected in the dimensionless fractional transport rates W_i^* plotted in Fig. 8. These provide some initial indication that larger transport rates are obtained for the coarse and fine size classes during the rising and falling limbs, respectively. However, it is informative to investigate how these different size classes are transported by comparing their fractional contribution f_{bi} to the overall and limb-separated bed load yields, with their relative abundance $f_{s\text{-}ini}$ in the initial bed sediment grading, for the full range of hydrograph conditions tested. Hence, Fig. 11 plots the fractional ratio $f_{bi}/f_{s\text{-}ini}$ versus the ratio W_k/Γ_{HG}, where $f_{bi}/f_{s\text{-}ini} > 1$ clearly represents the fractional bed load transport condition where size class *i* is transported at a proportionally higher level than found in the bed sediment grading (and vice versa).

Fig. 11(a) indicates that, during the rising limb of the design hydrographs, the ratio $f_{bi}/f_{s\text{-}ini} > 1$ for all medium size class yield data (i.e. $f_{bi}/f_{s\text{-}ini} = 1.15 – 1.49$) and virtual all fine size class yield data (i.e. $f_{bi}/f_{s\text{-}ini} = 0.93 – 1.24$), while relative mobility of the coarser size class is substantially lower (i.e. $f_{bi}/f_{s\text{-}ini} = 0.07 – 0.22$). It is noted that the fractional ratios for both the medium and coarse sizes tend to reduce as W_k/Γ_{HG} increases (i.e. through an increase in W_k and/or a reduction in Γ_{HG}), while the fine size class thus displays the opposite trend. These trends suggests that the medium and coarse size classes (corresponding to "gravel" sized grains) will mobilise more readily under flow hydrograph events with greater unsteadiness (even when smaller in magnitude), while the fine size class (corresponding to "sand" sized grains) will mobilise more readily under larger magnitude events with lower unsteadiness. However, it is clear that the level scatter on V1 and U1 series data indicates that the individual parametric influences of W_k and Γ_{HG} on the $f_{bi}/f_{s\text{-}ini}$ values during the rising limb are not entirely clear cut. By contrast, during the falling limb [Fig. 11(b)], the relative mobility of the fine size class (i.e. $f_{bi}/f_{s\text{-}ini} = 1.06 – 1.40$) is generally higher than the medium size class (i.e. $f_{bi}/f_{s\text{-}ini} = 0.99 – 1.32$), while the coarser size class mobility is also typically reduced compared to the rising limb (i.e. $f_{bi}/f_{s\text{-}ini} = 0.04 – 0.23$). Overall, all size classes show similar variation in $f_{bi}/f_{s\text{-}ini}$ with W_k/Γ_{HG} as was observed during the rising limbs [Fig. 11(a)] (i.e. indicative of increased mobilisation of fine sediment for higher magnitude events with lower unsteadiness and medium-coarse sediments during lower magnitude, more flashy events). These findings are consistent with the medium and coarse size classes having a preferential response on the rising limb, leading to mainly CW and N/M hysteresis patterns in bed load transport [Fig. 9(a) and (b)], and the fine size class having a preferential response on the falling limb, as indicated by the predominant N/M and CCW bed load hysteresis patterns [Fig. 9(c)].

Through a combined analysis of the fractional ratios over the entire design hydrographs [Fig. 11(c)] and during the separate rising and falling limbs, it can be deduced that, under zero-sediment supply conditions imposed, coarse grains exposed at the bed surface are most likely to be mobilised during the rising limbs, but also during the falling limb in highly flashy floods (i.e. hydrograph U3a-V3a, Table 1). However, the proportion of the coarse sized sediment in the overall bed load transport typically remains low compared to its relative proportion within the bed sediment. As the flow hydrographs become less unsteady (i.e. increasing durations and reducing peak flows), the proportions of fine and medium size classes in the overall bed load transport increase and reduce, respectively, whilst typically remaining well above their respective proportions in the bed sediment. As a consequence of this preferential transport, the bed surface grading tends to coarsen, leading to the formation of a surface armour layer that is commonly observed managed river reaches (i.e. downstream of a dam) [e.g. *Vericat et al*., 2006].

This post-hydrograph armoring of the bed surface layer is especially apparent at the upstream end of sediment bed test section and is thus representative of adjustments to bed load transport resulting from the disparity between limited upstream sediment supply and excess flow transport capacity [*Kondolf*, 1997; *Rinaldi and Simon*, 1998; *Simon and Rinaldi*, 2006; *Williams and Wolman*, 1984]. Progressive changes in the median bed surface grain size d_{s50} along the test bed section are typically characterised by significant coarsening (i.e. $d_{s50} >> d_{s50\text{-}ini}$) at the upstream end of the test bed (i.e. subject to zero-sediment feed from the inlet), with an asymptotic fining in d_{s50} values in the longitudinal direction (although remaining coarser than the overall bed sediment grading, i.e. $d_{s50} > d_{s50\text{-}ini}$). This exponential variability in bed surface median grain size e d_{s50} with downstream distance is well known from previous field and flume studies [*Morris and Williams*, 1999; *Paola et al.*, 1992; *Rice*, 1999;

Singer, 2008; *Ta et al.*, 2011], and can be expressed by considering the constant sediment sizes for long downstream distances as:

$$d_{s50}^{*} = k\,exp(-ax^{*}) + c \qquad (12)$$

where c is the post hydrograph median surface grain size d_{s50} at the downstream end of the reach (i.e. $x^{*} = x/L = 1$, with L = reach length) normalized by $d_{s50\text{-}ini}$ for the pre-event sediment bed grading, k is the normalized maximum value of d_{s50} at the upstream of the reach (i.e. $x = 0$), and a is a particle size diminution coefficient [*Parker et al.*, 2007]. At present, such exponential relationships were basically developed based on one individual survey over a short sediment sampling period. As such, the long-term variability in the size diminution coefficient a for a river reach or segment cannot be defined easily. In the current study, it is apparent from Fig. 7 that the extent of post-event bed surface coarsening at upstream end and the fining in the downstream direction is determined intrinsically by the total bed load yield W_t^{*} generated by each design hydrograph. Indeed, regression analysis shows k and a values to have a close relationship with W_t^{*} ($R^2 > 0.77$), such that:

$$k = 0.13\,ln(W_t^{*}) - 0.41 \qquad (R^2 = 0.77) \qquad (13a)$$

$$a = -5.54\,ln(W_t^{*}) + 53.20 \qquad (R^2 = 0.86) \qquad (13b)$$

Here, when more bed load sediment transport occurs along the test bed section, indicative of higher W_t^{*} values, the size diminution coefficient a decreases according to Eq. (13b). This matches, qualitatively at least, the field observations of *Luo et al*. [2012] in the middle and lower Yangtze River, where d_{s50} values had decreased at rates of 0.78 mm/km in 2008 and 0.20 mm/km in 2011 at the gravel–sand transition following the completion of the Three Gorges Dam in 2003. Within the current flume based study, this non-dimensional, exponential function (Eq. 12) and associated coefficients (Eq. 13) provide good agreement

with the longitudinal variability in d_{s50}^{*} along the test bed section for selected runs, with some localised deviations at more downstream locations [see Fig. 12(a)]. The model predictions from Eqs. (12) and (13) are also plotted in Fig. 12(b) for specific values of W_t^* (obtained by averaging design hydrograph runs that generate approximately equivalent total bed load yields W_t^*, see Table 2), showing good overall agreement with the measured bed surface coarsening along the test section. Finally, it is noted that the passage of design hydrograph events that yield very small W_t^* values will clearly generate minimal bed surface coarsening along the affected reach [as shown in Fig. 12(b) for $W_{t,ave}^{*}$= 240]. In fact, the degree of bed coarsening observed in these runs (i.e. d_{s50}^{*} > 1.1) may arise partly during initial bed sediment placement and partly as a consequence of bed surface rearrangement during antecedent flow conditions prior to the hydrograph event.

6 Conclusions

A flume study has been conducted to investigate the influence of unsteady hydrograph events on graded (sand/gravel) bed sediment transport properties and the resulting changes to bed surface composition, under zero-sediment feed conditions imposed at the upstream channel boundary. The design flow hydrographs were described quantitatively in terms of their shape (i.e. asymmetry η), unsteadiness Γ_{HG} and magnitude (i.e. total water work W_k), each of which were varied systematically to study the fractional bed load transport and bed surface responses under net bed degradation conditions.

Overall, it was found that the total water work W_k had largest influence on both the total and fractional bed load yields, followed by the unsteadiness Γ_{HG}, while hydrograph asymmetry η had little or no effect on bed load yields over the duration of the hydrographs. This finding was in general accord with previous related studies by the authors for both quasi-uniform (sand) and uni-/bi-modal (sand/gravel) sediments (*Wang et al*., 2015; 2019). In

the current study, two predictive bed load yield models, based on empirically-derived, combined hydrograph and bed sediment descriptors χ_{m1} and χ_{m2}, were both shown to reasonably collapse a wider range of experimental datasets for both graded (sand/gravel, sand/silt) and uniform (sand, gravel) bed sediments.

More detailed analysis of fractional bed load transport rates from the graded bed sediments throughout η, Γ_{HG} and W_k varied hydrographs confirmed that a temporal lag was displayed between the peak fractional transport rates for fine, medium and coarse size classes, with size-dependent hysteresis between the fractional bed load transport rates during the rising and falling hydrograph limbs. In particular, coarse particles were typically exposed at bed surface (at least partly due to bed surface rearrangement during antecedent flow conditions) and were more actively transported during the rising limb, resulting in a clockwise (CW) or no/mixed (N/M) transport hysteresis. By contrast, the more sheltered finer grain sizes tended to become more actively transported during the falling limb, leading to N/M or counterclockwise (CCW) hysteresis. Comparison with previous studies (*Wang et al.*, 2015; 2019) show that these hysteresis patterns were largely consistent over a wide range of design flow hydrographs, sediment mixtures and flume scales. Accordingly, the ratio of the bed load yields measured separately during the rising and falling hydrograph limbs for the coarse and medium sized sediment classes were normally greater than unity (i.e. $\psi_i > 1$), while the same bed yield ratio for the fine size class was typically close to or below unity (i.e. $\psi \leq 1$).

Accordingly, reference threshold shear stresses for the initiation and cessation of motion for the three size classes (fine, medium and coarse) during the design hydrographs revealed that lower threshold stress were required for the initiation of bed load transport during rising limb than were required for the cessation of transport during the falling limb for all three size classes. An improved predictive model for normalized fractional bed load

transport rates obtained under unsteady hydrograph flows, based on the separate-limb method proposed initially by *Waters and Curran* [2015], was therefore shown to fit better to these experimental measurements as it takes better account of differential bed load rates measured during the rising and falling limbs (i.e. associated with the observed CW, N/M and CCW hysteresis patterns for fractional bed load transport).

The variability in bed load composition during the design hydrographs was intrinsically controlled by the upstream sediment supply condition, the bed sediment grading and the design hydrograph characteristics. Specifically, if the hydrograph was short in duration with a lower peak flow (i.e. lower W_k) the zero-sediment supply condition imposed at the upstream channel inlet had no significant effect on non-equilibrium sediment transport, with the median size d_{b50} of the bed load transport remaining relatively invariable over the hydrograph duration. However, when the hydrograph peak flow and duration increased (i.e. higher W_k), the zero-sediment supply condition led to a general coarsening of the bed load during the rising limb followed by a distinct fining during the falling limb. An overall reduction in unsteadiness Γ_{HG} (i.e. through a combined reduction in peak flow and increase in the hydrograph duration) was also shown to result in a monotonic reduction in the bed load d_{b50} throughout the hydrograph. Analysis of the fractional bed load composition obtained over all symmetrical design flow hydrographs indicated that the coarser gravels were more easily mobilized under flashier hydrographs (i.e. events with higher unsteadiness Γ_{HG}). This demonstrates strong correlation to the transport of large bed elements, such as cobbles or boulders, by short-lived flash flood events that occur frequently in mountain streams and rivers. Furthermore, we observed that these coarser sediment grains were more susceptible to mobilisation during by rising limb, even though their overall proportion in the total bed load transport remained relatively low and decreased further as the flow hydrographs became less flashy (i.e. through reducing unsteadiness Γ_{HG}). These changes were largely due to the impact

of the non-equilibrium sediment transport generated under the imposed zero-sediment supply condition, with coarse sediments becoming increasingly difficult to mobilise from the bed under unsteady flow hydrographs with reduced peak flows and longer overall durations.

Finally, post-hydrograph measurements of the bed surface composition showed that the transport of graded bed sediments under the design flow hydrographs, in the absence of sediment feed from the upstream end, resulted in an overall coarsening (i.e. armouring) of the bed surface layer. More specifically, the spatial variation in median bed surface grain size d_{s50} along the length of the test bed section showed significant coarsening at the upstream end of the channel with an asymptotic decrease in d_{s50} in the upper to mid-section of the test bed (i.e. the transition region), with d_{s50} remaining approximately constant, but still slightly coarsened, at more downstream locations. It was also found that the upstream bed coarsening increased as total water work W_k and unsteadiness Γ_{HG} increased, while the gradual fining in the downstream direction was well represented by an empirical exponential model.

Acknowledgments and data access

This work was also supported financially by the Fundamental Research Funds for the Central Universities (Grant No. 2020MS024). The experimental data used in this study is available in Dr Le Wang's PhD thesis entitled "*Bed-load Sediment Transport and Bed Evolution in Steady and Unsteady Flows*", available at http://www.ros.hw.ac.uk/handle/10399/3099.

References

Berta, A. M., Bianco, G. (2010). An expression for the water-sediment moving layer in unsteady flows valid for open channels and embankments. Natural Hazards and Earth Systems Sciences, 10(5), 1051-1059. https://doi.org/10.5194/nhess-10-1051-2010.

Bombar, G., Elçi, Ş., Tayfur, G., Güney, M. Ş., Bor, A. (2011). Experimental and Numerical Investigation of Bed-Load Transport under Unsteady Flows, Journal of Hydraulic Engineering (ASCE). 137(10), 1276-1282. https://doi.org/10.1061/(ASCE)HY.1943-7900.0000412.

Einstein, H. A. (1942). Formulas for the transportation of bed load. Transactions of the American Society of Civil Engineers, 107(1), 561-577.

Frey, P., Ducottet, C., Jay, J. (2003). Fluctuations of bed load solid discharge and grain size distribution on steep slopes with image analysis. Experiments in Fluids, 35(6), 589-597. DOI 10.1007/s00348-003-0707-9.

Graf, W. H., Suszka, L. (1985). Unsteady flow and its effect on sediment transport. Proceedings of 21st IAHR Congress, pp. 1-5, Melbourne, Australia.

Guney, M. S., Bombar, G., Aksoy, A. O. (2013). Experimental Study of the Coarse Surface Development Effect on the Bimodal Bed-Load Transport under Unsteady Flow Conditions. Journal of Hydraulic Engineering (ASCE), 139(1), 12-21. https://doi.org/10.1061/(ASCE)HY.1943-7900.0000640

Hassan, M. A., Egozi, R., Parker, G. (2006). Experiments on the effect of hydrograph characteristics on vertical grain sorting in gravel bed rivers. Water Resources Research, 42(9), W09408. https://doi.org/10.1029/2005WR004707.

Hassan, W. N., Ribberink, J. S. (2005). Transport processes of uniform and mixed sands in oscillatory sheet flow. Coastal Engineering, 52(9), 745-770. https://doi.org/10.1016/j.coastaleng.2005.06.002.

Humphries, R., Venditti, J. G., Sklar, L. S., Wooster, J. K. (2012). Experimental evidence for the effect of hydrographs on sediment pulse dynamics in gravel- bedded rivers. Water Resources Research, 48, W01533. https://doi.org/10.1029/2011WR010419.

Kondolf, G. M. (1997). Hungry water: Effects of dams and gravel mining on river channels. Environmental Management, 21(4), 533–551. https://doi.org/10.1007/s002679900048.

Kuhnle, R. A., Southard, J. B. (1988). Bed load transport fluctuations in a gravel bed laboratory channel. Water Resources Research, 24(2), 247-260. https://doi.org/10.1029/WR024i002p00247.

Lee, H., Balachandar S. (2012). Critical shear stress for incipient motion of a particle on a rough bed. Journal of Geophysical Research (Earth Surface), 117, 1026. https://doi.org/10.1029/2011JF002208.

Lee, K. T., Liu, Y. L., Cheng, K. H. (2004). Experimental investigation of bedload transport processes under unsteady flow conditions. Hydrological Processes, 18(13), 2439-2454. https://doi.org/10.1002/hyp.1473.

Luo, X., Yang S., Zhang, J. (2012). The impact of the Three Gorges Dam on the downstream distribution and texture of sediments along the middle and lower Yangtze River (Changjiang) and its estuary, and subsequent sediment dispersal in the East China Sea, Geomorphology, 179, 126-140. https://doi.org/10.1016/j.geomorph.2012.05.034.

Mao, L. (2012). The effect of hydrographs on bed load transport and bed sediment spatial arrangement. Journal of Geophysical Research, 117, F03024. https://doi.org/10.1029/2012JF002428.

Misri, R. L., Garde, R. J., Raju, K. G. R. (1984). Bed load transport of coarse nonuniform sediment, Journal of Hydraulic Engineering, 110(3), 312-328. https://doi.org/10.1061/(ASCE)0733-9429(1984)110:3(312).

Morris, P., Williams, D. (1999). A worldwide correlation for exponential bed particle size variation in subaerial aqueous flows. Earth Surface Processes and Landforms, 24(9), 835-847. https://doi.org/10.1002/(SICI)1096-9837(199908)24:9<835::AID-ESP15>3.0.CO;2-G.

Ockelford, A. M., Haynes, H. (2013). The impact of stress history on bed structure. Earth Surface Processes and Landforms, 38(7), 717-727. https://doi.org/10.1002/esp.3348.

Paola, C., Parker, G., Seal, R., Sinha, S. K., Southard, J. B., Wilcock, P. R. (1992). Downstream fining by selective deposition in a laboratory flume, Science, 258(5089), 1757-1760. DOI: 10.1126/science.258.5089.1757.

Parker, G., Klingeman, P. C., McLean, D. G. (1982). Bedload and size distribution in paved gravel-bed streams, Journal of the Hydraulics Division (ASCE), 108(4), 544-571. https://doi.org/10.1061/(ASCE)0733-9429(1983)109:5(793).

Parker, G., Hassan, M., Wilcock, P. (2007). Adjustment of the bed surface size distribution of gravel-bed rivers in response to cycled hydrographs. Developments in Earth Surface Processes, 11, 241-285. https://doi.org/10.1016/S0928-2025(07)11127-5.

Patel, P. L., Ranga Raju, K. G. (1996). Fractionwise calculation of bed load transport. Journal of Hydraulic Research, 34(3), 363-379. https://doi.org/10.1080/00221689609498485.

Phillips, B. C., Sutherland, A. J. (1990). Temporal lag effect in bed load sediment transport. Journal of Hydraulic Research, 28(1), 5-23. https://doi.org/10.1080/00221689009499144.

Piedra, M. M. (2010). Flume investigation of the effects of sub-threshold rising flows on the entrainment of gravel beds. PhD thesis, University of Glasgow.

Recking, A., Frey, P., Paquier, A., Belleudy, P. (2009). An experimental investigation of mechanisms involved in bed load sheet production and migration. Journal of Geophysical Research (Earth Surface), 114(F3). https://doi.org/10.1029/2008JF000990.

Rice, S. (1999). The nature and controls on downstream fining within sedimentary links. Journal of Sedimentary Research, 69(1), 32-39. https://doi.org/10.2110/jsr.69.32.

Rinaldi, M., Simon, A. (1998). Bed- level adjustments in the Arno River, central Italy. Geomorphology, 22(1), 57–71. https://doi.org/10.1016/S0169-555X(97)00054-8.

Saadi, Y. (2002). The influence of different time varying antecedent flows on the stability of mixed grain size deposits. PhD thesis, University of Sheffield.

Samaga, B. R., Ranja Raju, K. G., Garde, R. J. (1986). Bed Load Transport of Sediment Mixtures. Journal of Hydraulic Engineering (ASCE), 112(11), 1003-1017. https://doi.org/10.1061/(ASCE)0733-9429(1986)112:11(1003).

Simon, A., Rinaldi, M. (2006). Disturbance, stream incision, and channel evolution: The roles of excess transport capacity and boundary materials in controlling channel response. *Geomorphology*, *79*(3), 361-383. https://doi.org/10.1016/j.geomorph.2006.06.037.

Singer, M. B. (2008). Downstream patterns of bed material grain size in a large, lowland alluvial river subject to low sediment supply. Water Resources Research, 44(12), W12202, https://doi.org/10.1029/2008WR007183.

Suszka, U. L. (1987), Sediment transport at steady and unsteady flow, PhD thesis, EPFL.

Ta, W., Wang, H., Jia, X. (2011). Downstream fining in contrasting reaches of the sand-bedded Yellow River. Hydrological Processes, *25*(24), 3693-3700. https://doi.org/10.1002/hyp.8065.

Vericat, D., Batalla, R. J., Garcia, C. (2006). Break-up and reestablishmnet of the armour layer in a large gravel-bed tiver below dams: The lower Ebro. Geomorphology, 76, 122-136. https://doi.org/10.1016/j.geomorph.2005.10.005.

Wang, L. (2016). Bedlaod sediment transport and bed evolution in steady and unsteady flows. PhD thesis, Heriot-Watt University.

Wang, L., Cuthbertson, A. J. S., Pender, G., Cao, Z. (2015). Experimental investigations of graded sediment transport under unsteady flow hydrographs. International Journal of Sediment Research, 30(4), 306-320. https://doi.org/10.1016/j.ijsrc.2015.03.010.

Wang, L., Cuthbertson, A. J. S., Pender, G., Zhong, D. (2019). Bed load sediment transport and morphological evolution in a degrading uniform sediment channel under unsteady flow

hydrographs. Water Resources Research, 55, 5431–5452. https://doi.org/10.1029/2018WR024413.

Waters, K. A., Curran, J. C. (2015). Linking bed morphology changes of two sediment mixtures to sediment transport predictions in unsteady flows. Water Resources Research, 51(4), 2724-2741. https://doi.org/10.1002/2014WR016083.

Wilcock, P. R., McArdell, B. W. (1993). Surface-based fractional transport rates: Mobilization thresholds and partial transport of a sand-gravel sediment. Water Resources Research, 29(4), 1297-1312. https://doi.org/10.1029/92WR02748.

Wilcock, P. R., Kenworthy, S. T., Crowe, J. C. (2001). Experimental study of the transport of mixed sand and gravel. Water Resources Research, 37(12), 3349-3358. https://doi.org/10.1029/2001WR000683.

Wilcock, P. R., Crowe, J. C. (2003). Surface-based transport model for mixed-size sediment. Journal of Hydraulic Engineering, 129(2), 120-128. https://doi.org/10.1061/(ASCE)0733-9429(2003)129:2(120).

Wilcock, P. R., DeTemple, B. T. (2005). Persistence of armor layers in gravel-bed streams. Geophysical Research Letters, 32(8). https://doi.org/10.1029/2004GL021772.

Williams, G. P. (1989). Sediment concentration versus water discharge during single hydrologic events in rivers. Journal of Hydrology, 111(1), 89-106. https://doi.org/10.1016/0022-1694(89)90254-0.

Williams, G. P., Wolman, M. G. (1984). Downstream effects of dams on alluvial rivers. USGS report 1286. https://doi.org/10.3133/pp1286.

Yen, C.L., Lee, K. T. (1995). Bed topography and sediment sorting in channel bend with unsteady flow. Journal of Hydraulic Engineering (ASCE), 121(8), 591-599. https://doi.org/10.1061/(ASCE)0733-9429(1995)121:8(591).

Figure Captions

Figure 1. Schematic representation of flume channel and experimental set-up.

Figure 2. Graded bed sediment mixture and fractional grain size classes considered in the present experiment.

Figure 3. Example plots showing temporal variation in total and fractional (fine, medium and coarse size classes) bed load transport rates q_b with flow rate Q for runs (a) S1a (U1a, V1a), (b) S1b, (c) U1d and (d) V1d (see Table 1).

Figure 4. Example hysteresis plots of total and fractional (fine, medium and coarse size classes) bed load transport versus flow rate Q for runs (a) S1a (U1a, V1a), (b) S1b, (c) U1d and (d) V1d (see Table 1).

Figure 5. Individual and combined effects of hydrograph-related parameters: (a) total water work W_k, (b) unsteadiness Γ_{HG}, and (c) combined hydrograph descriptor $\xi_g = W_k\Gamma_{HG}^{0.63}$ on the total and fractional bed load yields W_t^* and W_{ti}^* from graded bed sediment transport.

Figure 6. Temporal variations in bed load median grain size d_{b50} over the duration of (a-c) η-varying (i.e. group S1, Table 1), (b) Γ_{HG}-varying (i.e. group U1, Table 1) and (c) W_k-varying (i.e. group V1, Table 1) design hydrographs.

Figure 7. Measured post hydrograph bed surface median grain size d_{s50} along the bed test section for (a) η-varying (i.e. group S1, Table 1), (b) Γ_{HG}-varying (i.e. group U1, Table 1), and (c) W_k-varying (i.e. group V1, Table 1) design hydrographs. Part (d) shows the variation in the post hydrograph normalised bed surface grain size $d_{s0}^* = d_{s50}/d_{s50\text{-}ini}$ at $x = 0$ with combined hydrograph parameter $\xi_g = W_k\Gamma_{HG}^{0.63}$.

Figure 8. Dimensionless fractional bed load transport W_i^* versus Shields stress ratio τ^*_{bi}/τ^*_{bir} for (a) total hydrograph, (b) rising limb, and (c) falling limb data. [Note: fit to Eq. (10) represented by solid lines with best fit regression to datasets shown as dashed trend lines].

Figure 9. Summary of bed load transport hysteresis patterns and corresponding bed load yield ratio ψ_{ti} for (a-c) coarse, medium and fine size classes and (d) total bed sediment grading plotted within the W_k: Γ_{HG} domain space.

Figure 10. Total bed load yields W_t^* plotted as a function of combined hydrograph-bed sediment descriptors (a) $\chi_{m1} = W_k\Gamma_{HG}^{0.63}(H_p/d_{50})^{2.5}$ and (b) $\chi_{m2} = W_k\Gamma_{HG}^{0.2}(H_p/d_{50})^{2.5}$ showing overall level of agreement with data from the current study and similar data from previous studies considering both uniform and graded bed sediments.

Figure 11. Variability in relative proportional representation $f_{bi}/f_{s\text{-}ini}$ for three size classes in the bed load transport yields measured over (a) rising limb, (b) falling limb, and (c) overall hydrograph for varying ratios of total water work W_k to unsteadiness Γ_{HG} for symmetrical design flow hydrographs.

Figure 12. Variation of post hydrograph normalised bed surface grain size d_{s50}^* with downstream distance $x^* = x/L$ showing best fit exponential model predictions (from Eqs. 12 and 13) for (a) individual, selected experimental runs (as shown), and (b) run-averaged data based on specific W_k values.

Table Captions

Table 1. Unsteady design flow hydrograph conditions and bed load sampling intervals.

Table 2. Summary of main bed load sediment transport characteristics under unsteady design hydrograph flows (see Table 1).

Figure1

Figure 1.

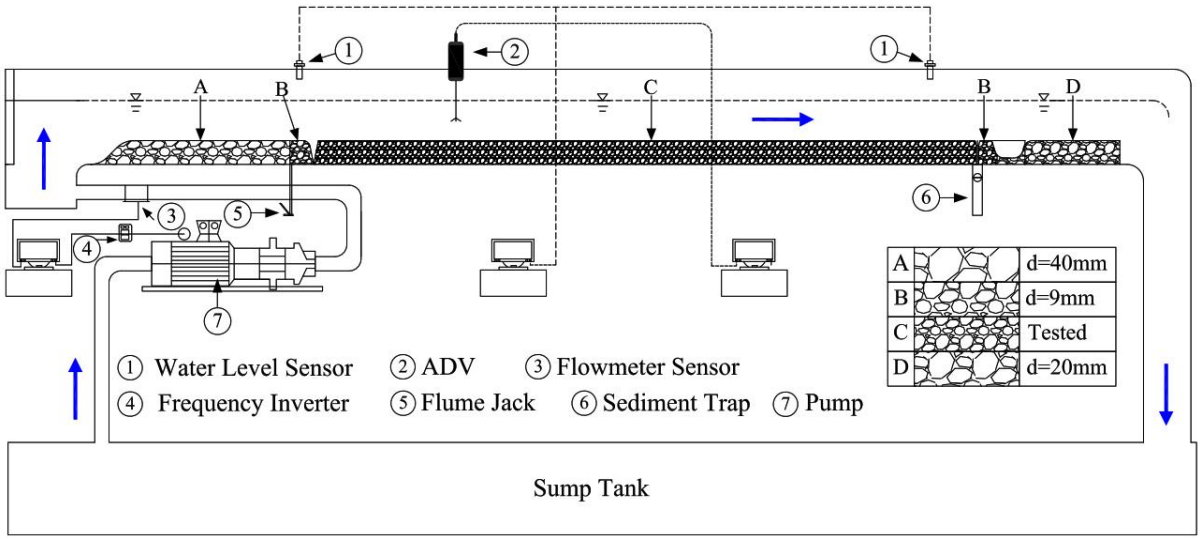

Figure2

Figure 2.

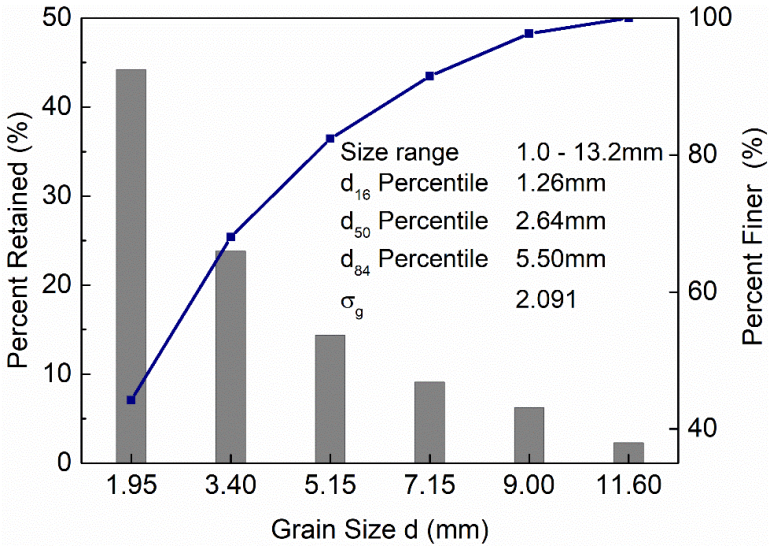

Size Class	d_i (mm)	d_{50i} (mm)
Fine	1.0 – 2.8	1.95
Medium	2.8 – 6.3	4.0
Coarse	6.3 – 13.2	9.0

Figure3

Figure 3.

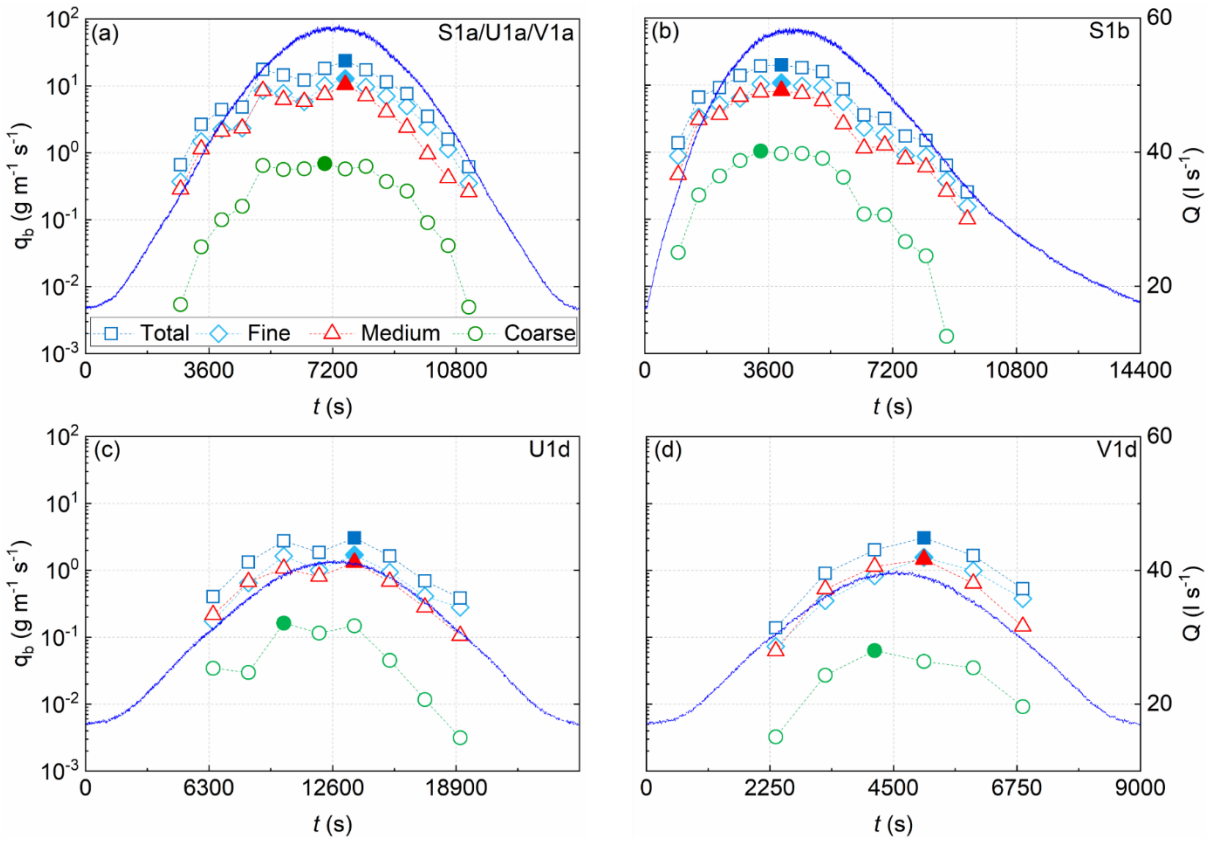

Figure4

Figure 4.

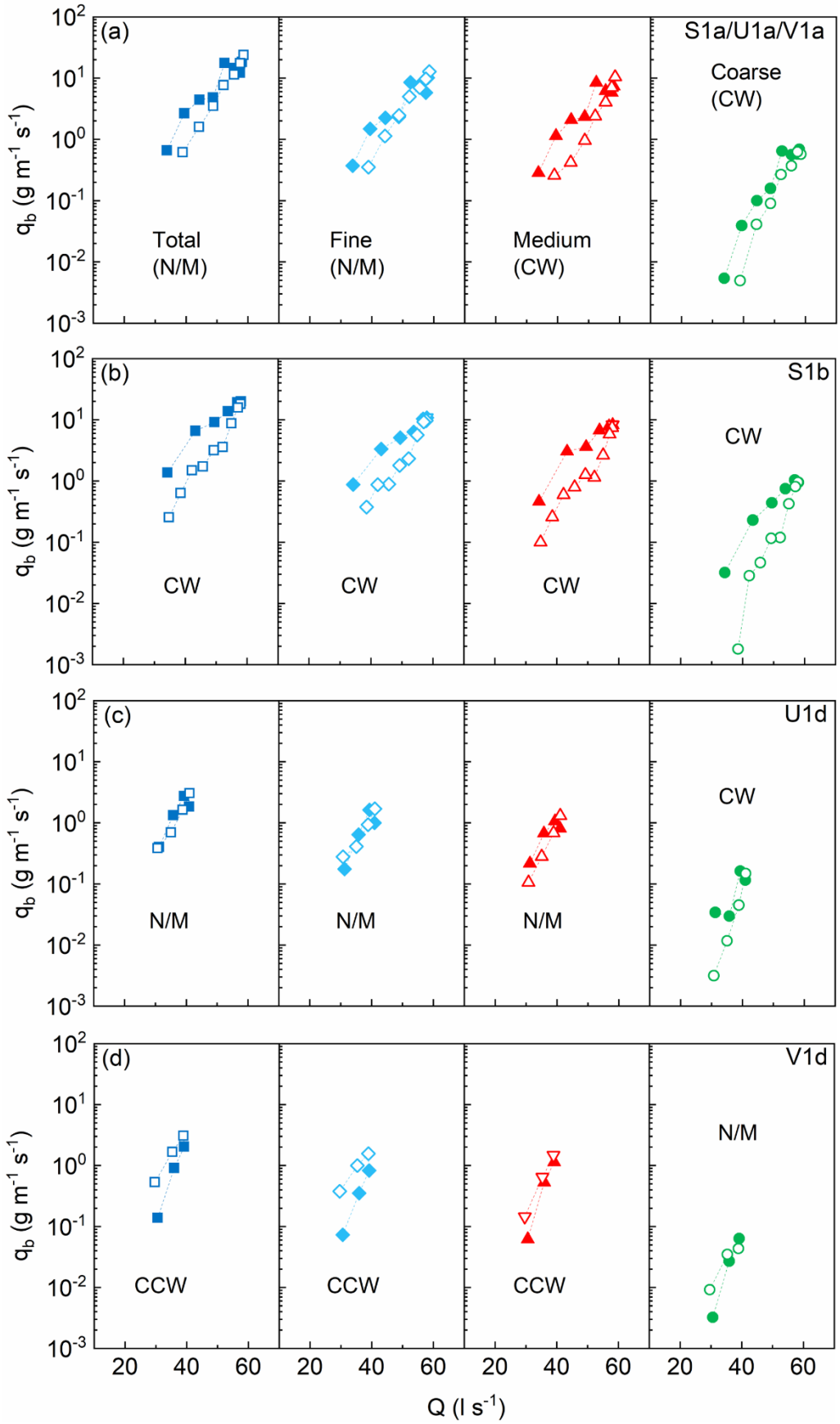

Figure 5.

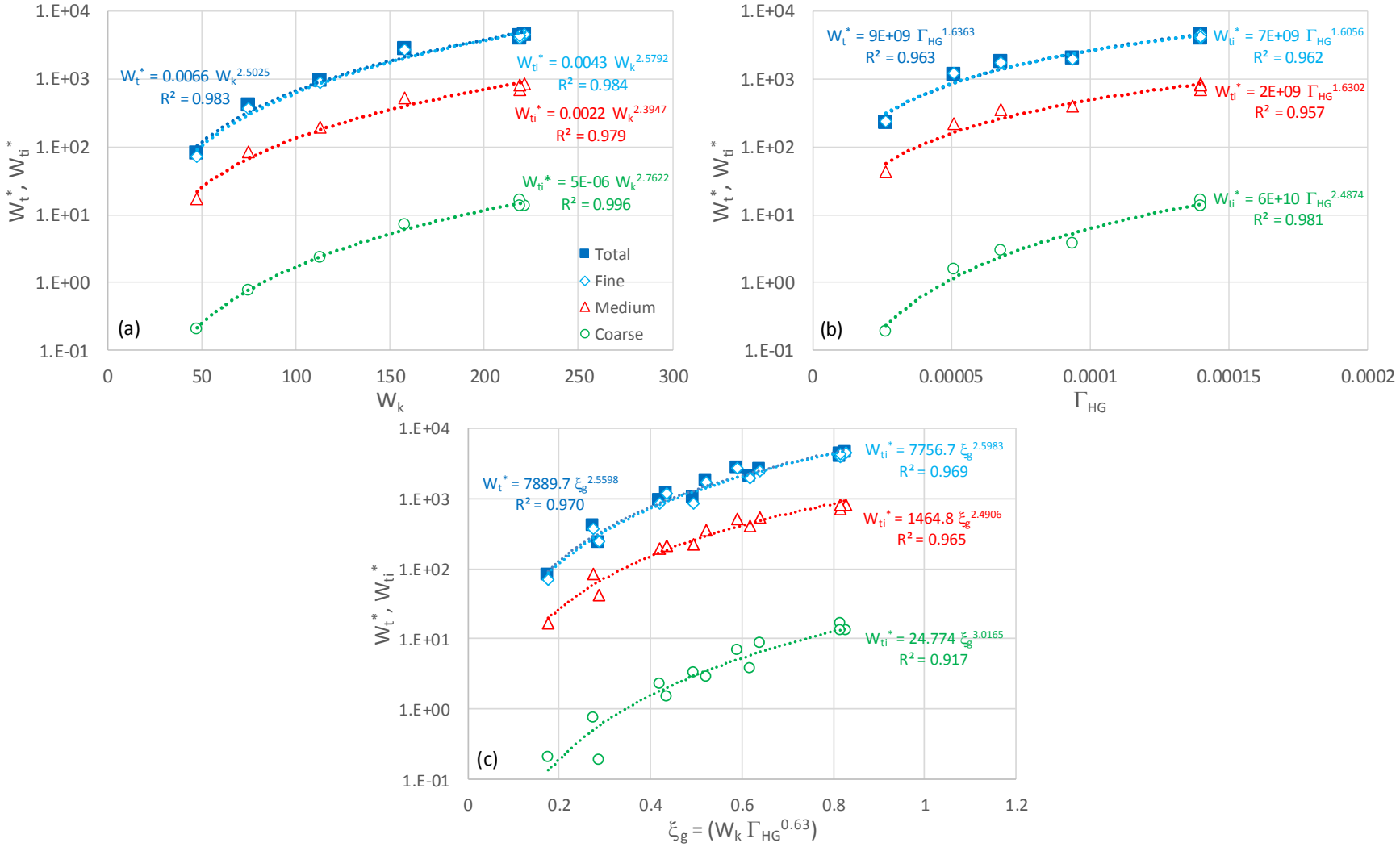
(a)
$W_t^* = 0.0066\ W_k^{2.5025}$
$R^2 = 0.983$
$W_{ti}^* = 0.0043\ W_k^{2.5792}$
$R^2 = 0.984$
$W_{ti}^* = 0.0022\ W_k^{2.3947}$
$R^2 = 0.979$
$W_{ti}^* = 5E\text{-}06\ W_k^{2.7622}$
$R^2 = 0.996$
Total
Fine
Medium
Coarse
W_t^*, W_{ti}^*
W_k
(b)
$W_t^* = 9E+09\ \Gamma_{HG}^{1.6363}$
$R^2 = 0.963$
$W_{ti}^* = 7E+09\ \Gamma_{HG}^{1.6056}$
$R^2 = 0.962$
$W_{ti}^* = 2E+09\ \Gamma_{HG}^{1.6302}$
$R^2 = 0.957$
$W_{ti}^* = 6E+10\ \Gamma_{HG}^{2.4874}$
$R^2 = 0.981$
Γ_{HG}
(c)
$W_t^* = 7889.7\ \xi_g^{2.5598}$
$R^2 = 0.970$
$W_{ti}^* = 7756.7\ \xi_g^{2.5983}$
$R^2 = 0.969$
$W_{ti}^* = 1464.8\ \xi_g^{2.4906}$
$R^2 = 0.965$
$W_{ti}^* = 24.774\ \xi_g^{3.0165}$
$R^2 = 0.917$
$\xi_g = (W_k\ \Gamma_{HG}^{0.63})$

Figure6

Figure 6.

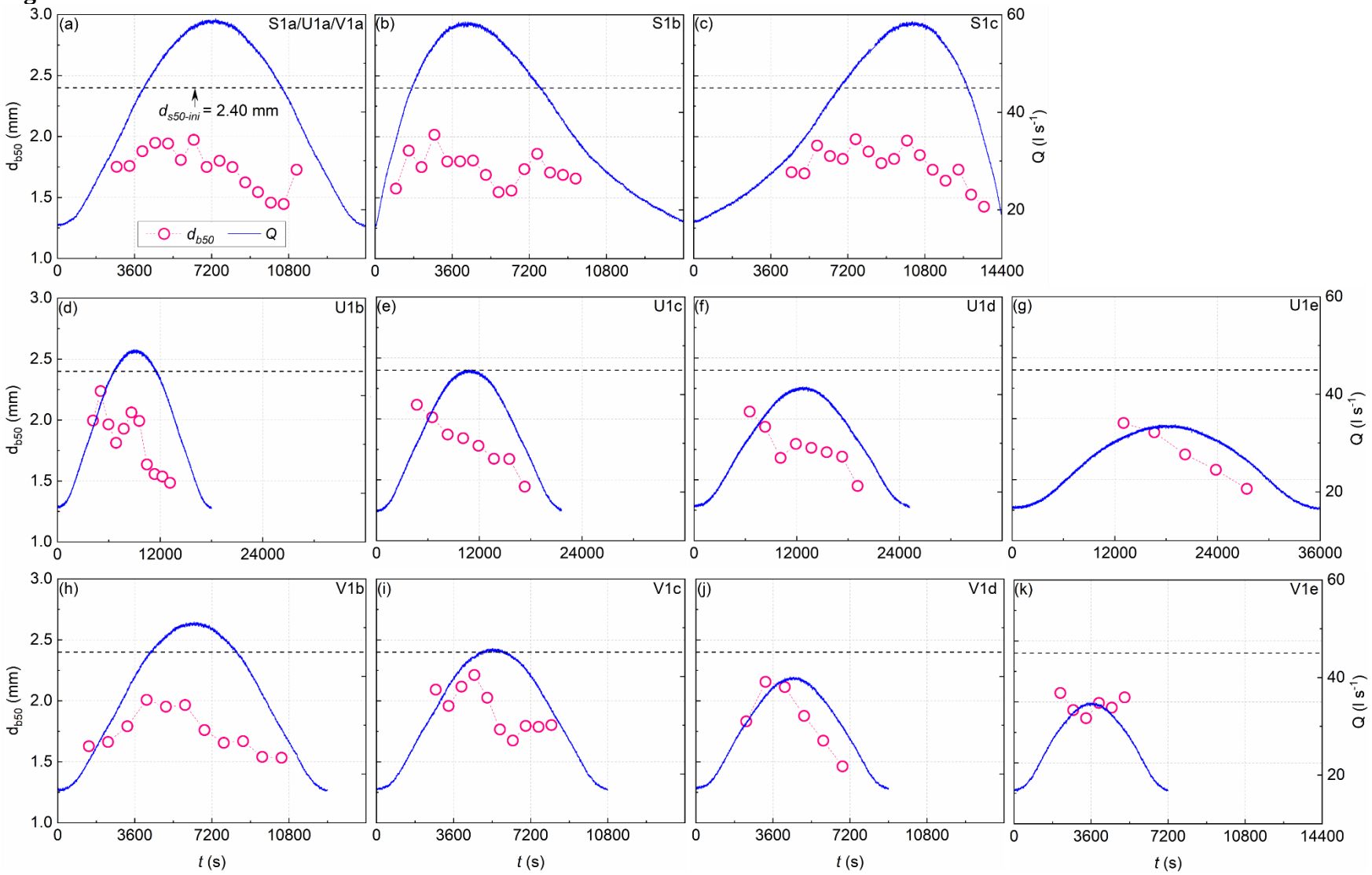

Figure 7.

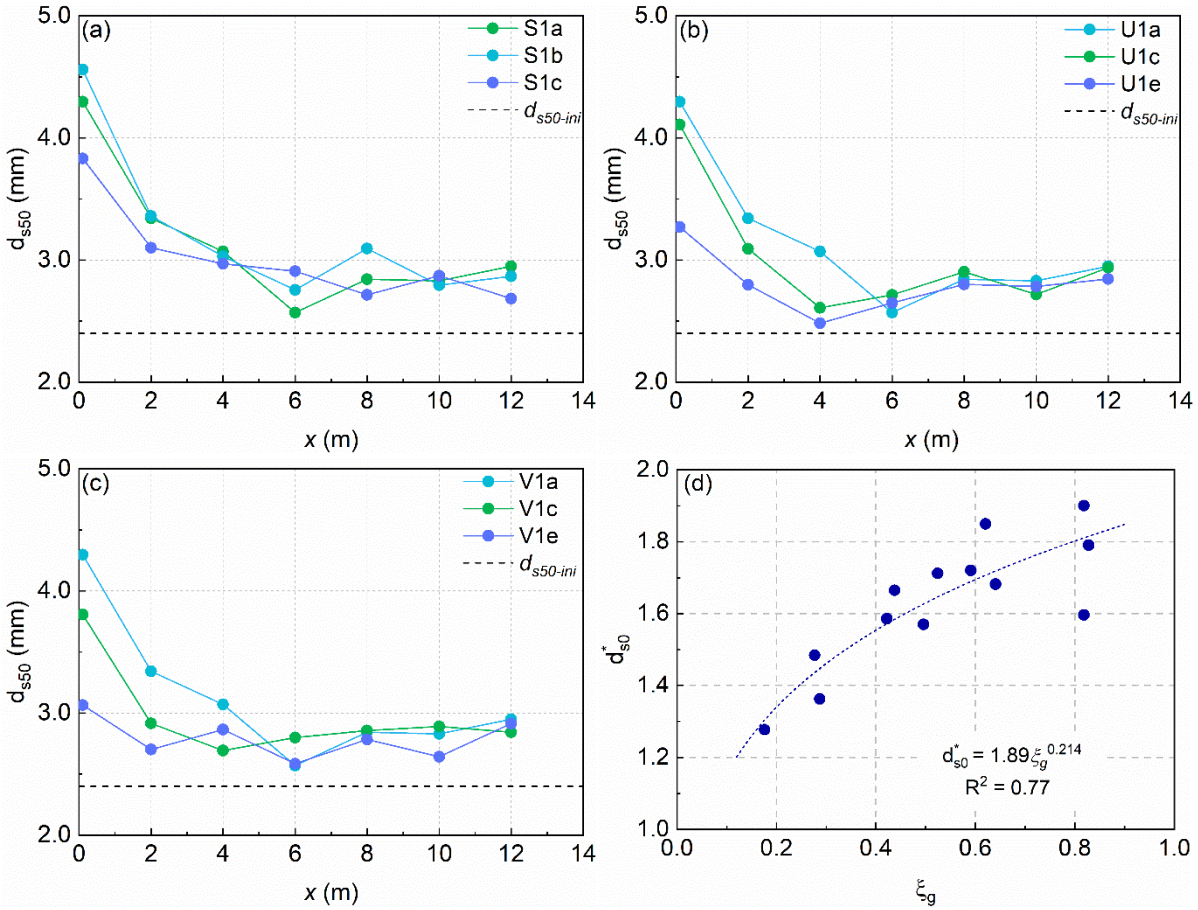
(a)
S1a
S1b
S1c
$d_{s50\text{-}ini}$
d_{s50} (mm)
x (m)
(b)
U1a
U1c
U1e
$d_{s50\text{-}ini}$
d_{s50} (mm)
x (m)
(c)
V1a
V1c
V1e
$d_{s50\text{-}ini}$
d_{s50} (mm)
x (m)
(d)
$d^*_{s0} = 1.89\xi_g^{0.214}$
$R^2 = 0.77$
d^*_{s0}
ξ_g

Figure8

Figure 8:

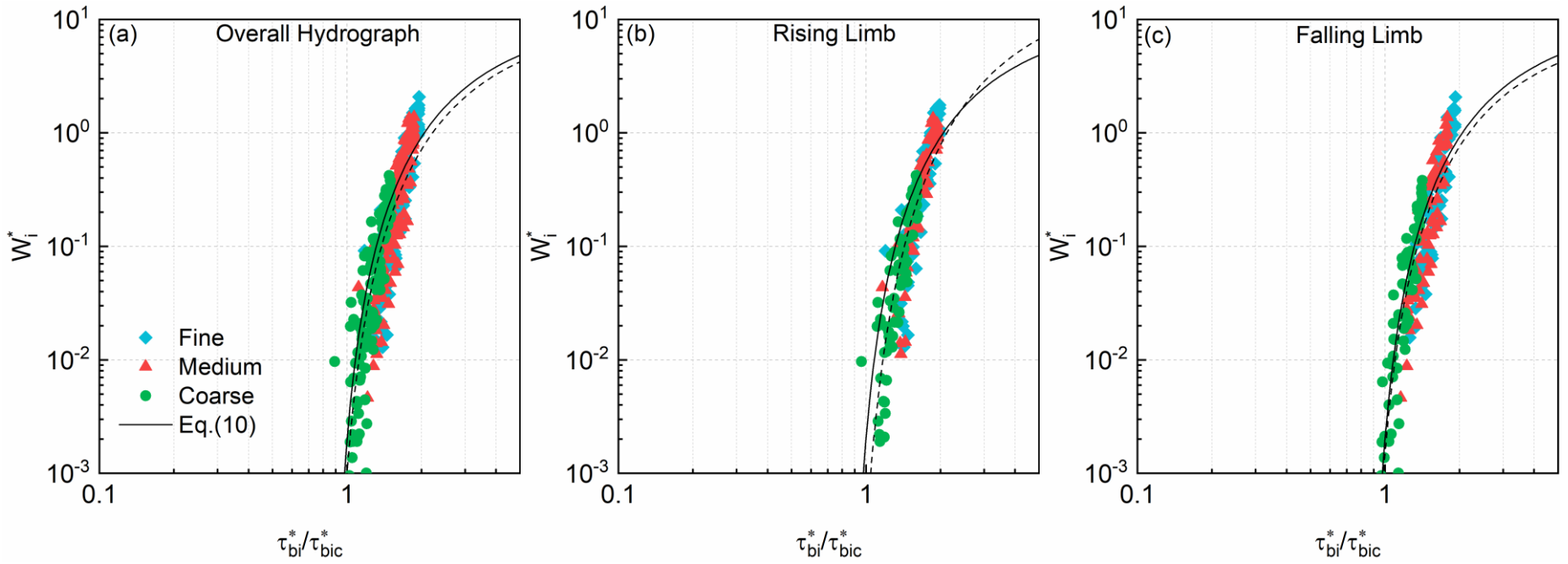

Figure9

Figure 9:

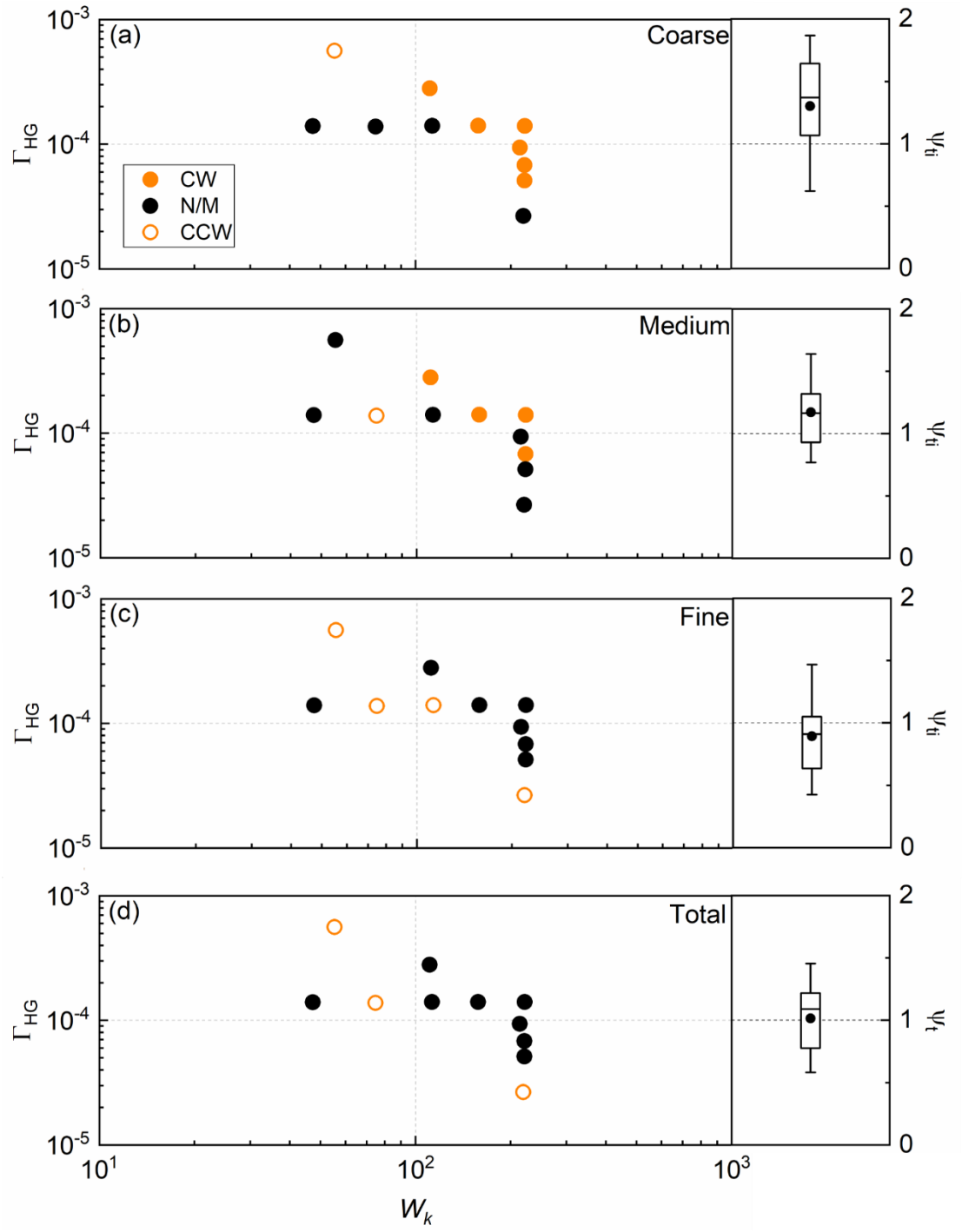

Figure10

Figure 10.

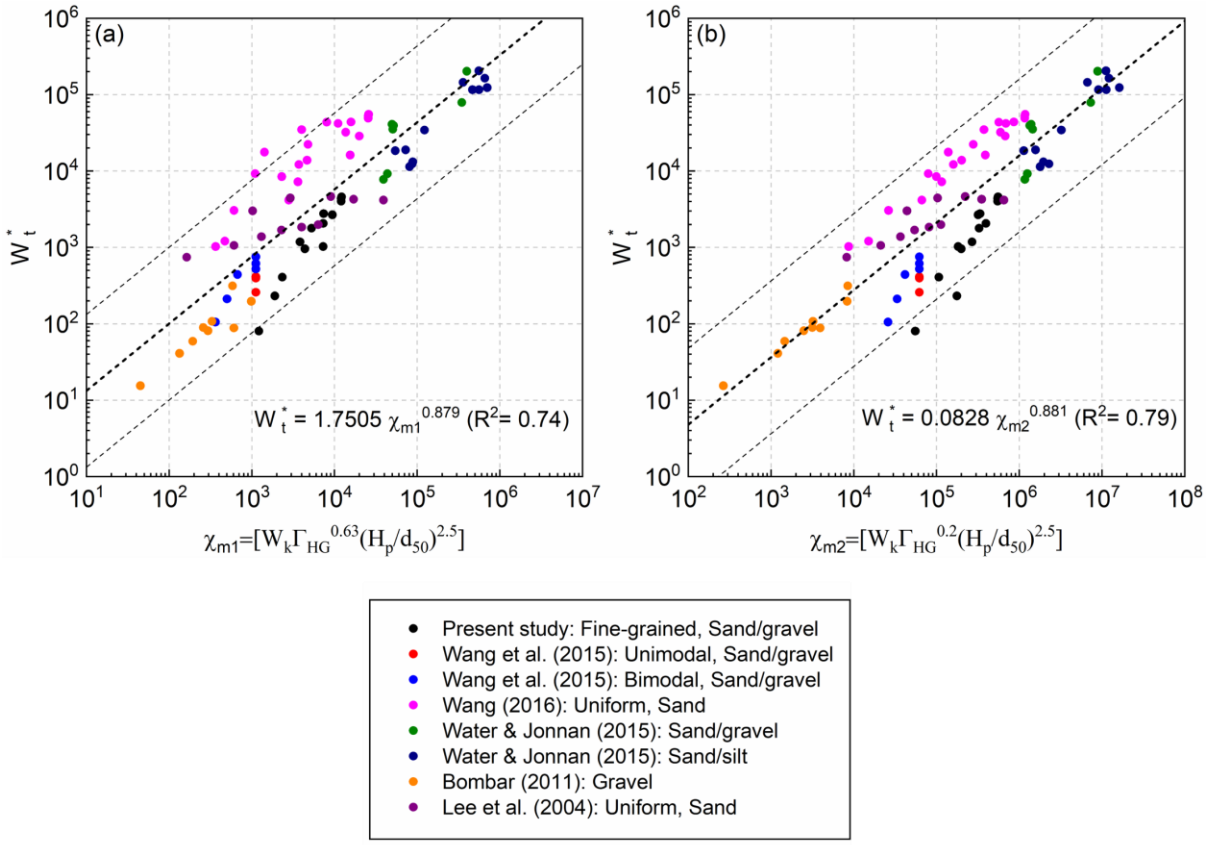

Figure11

Figure 11.

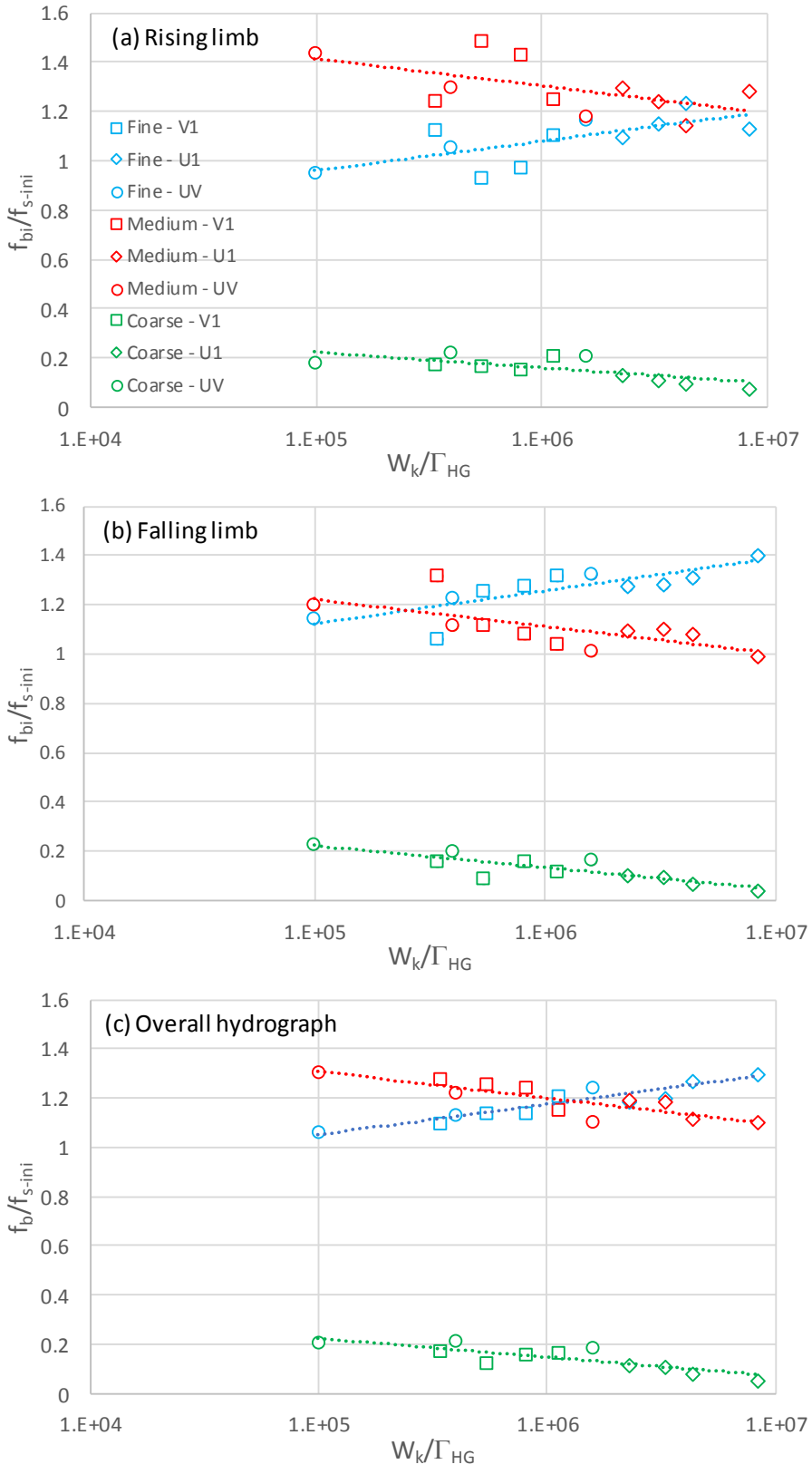

Figure12

Figure 12.

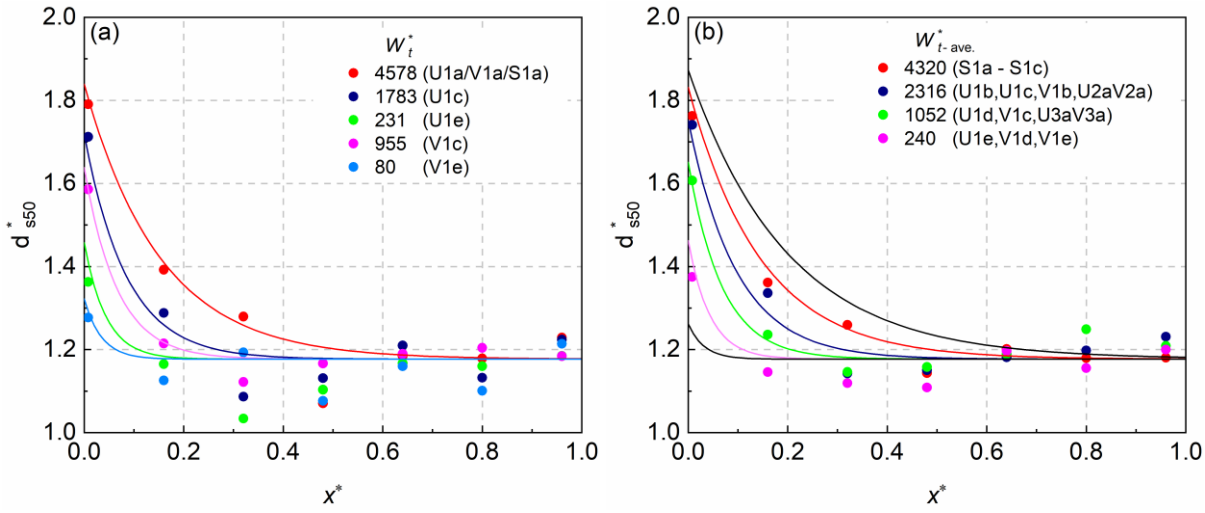

Table1
Click here to download Table: Table1.docx

Table 1. Unsteady design flow hydrograph conditions and bed load sampling intervals.

Group	Run No.	Q_p (l·s^{-1})	H_p (m)	ΔT_R (s)	ΔT_F (s)	ΔT (s)	Γ_{HG} ($\times 10^{-4}$)	W_k	η	Sampling intervals (s)
	S1a	58.0	0.1228	7200	7200	14400	1.400	221.76	1.0	600
S1	S1b	58.0	0.1228	4114	10286	14400	1.400	219.13	0.4	600
	S1c	58.0	0.1228	10286	4114	14400	1.400	219.13	2.5	600
	V1a	58.0	0.1228	7200	7200	14400	1.400	221.76	1.0	600
	V1b	52.0	0.1150	6300	6300	12600	1.405	157.94	1.0	900
V1	V1c	46.0	0.1069	5400	5400	10800	1.402	112.94	1.0	600
	V1d	40.0	0.0983	4500	4500	9000	1.381	74.78	1.0	900
	V1e	35.0	0.0908	3600	3600	7200	1.395	47.32	1.0	600
	U1a	58.0	0.1228	7200	7200	14400	1.400	221.76	1.0	600
	U1b	50.0	0.1124	9000	9000	18000	0.937	214.02	1.0	900
U1	U1c	45.0	0.1055	10800	10800	21600	0.680	221.24	1.0	1800
	U1d	41.0	0.0998	12600	12600	25200	0.512	221.12	1.0	1800
	U1e	34.0	0.0892	18000	18000	36000	0.265	219.18	1.0	3600
	U1a-V1a	58.0	0.1228	7200	7200	14400	1.400	221.76	1.0	600
UV	U2a-V2a	58.0	0.1228	3600	3600	7200	2.801	110.88	1.0	600
	U3a-V3a	58.0	0.1228	1800	1800	3600	5.602	55.44	1.0	300

Table2
Click here to download Table: Table2.docx

Table 2. Summary of main bed load sediment transport characteristics under unsteady design hydrograph flows (see Table 1).

Group	Run No.	$q_{b,max}$ (g m^{-1} s^{-1})				Bed-load transport hysteresis				Bed-load yields W_t^*, W_{ti}^*				Bed-load yields ratio ψ_t, ψ_{ti}			
		Total	Fine	Medium	Coarse	Total	Fine	Medium	Coarse	Total	Fine	Medium	Coarse	Total	Fine	Medium	Coarse
S1	S1a	23.77	12.80	10.39	0.69	N/M	N/M	CW	CW	4577.6	4589.4	836.1	13.27	1.14	1.00	1.32	1.41
	S1b	19.99	10.77	8.27	1.04	CW	CW	CW	CW	4013.2	4031.7	705.9	16.61	1.31	1.19	1.50	1.38
	S1c	17.67	9.85	7.37	0.68	CW	CW	CW	CW	4369.3	4259.2	818.5	13.66	1.78	1.60	2.03	1.75
V1	V1a	23.77	12.80	10.39	0.69	N/M	N/M	CW	CW	4577.6	4589.4	836.1	13.27	1.14	1.00	1.32	1.41
	V1b	13.55	7.53	5.82	0.42	N/M	N/M	CW	CW	2760.0	2690.5	526.7	7.14	1.09	0.91	1.31	1.87
	V1c	8.26	4.57	3.67	0.19	N/M	CCW	N/M	N/M	955.0	876.7	196.0	2.31	0.83	0.63	1.10	0.80
	V1d	3.08	1.57	1.47	0.06	CCW	CCW	CCW	N/M	407.7	375.1	84.6	0.76	0.58	0.43	0.77	1.07
	V1e	0.68	0.35	0.32	0.03	N/M	N/M	N/M	N/M	80.0	70.8	16.9	0.21	1.39	1.47	1.31	1.50
U1	U1a	23.77	12.80	10.39	0.69	N/M	N/M	CW	CW	4577.6	4589.4	836.1	13.27	1.14	1.00	1.32	1.41
	U1b	8.60	4.93	4.47	0.17	N/M	N/M	N/M	CW	2055.2	1972.8	407.2	3.80	0.95	0.82	1.12	1.16
	U1c	5.59	3.07	2.50	0.32	N/M	N/M	CW	CW	1783.2	1732.2	350.1	2.96	1.46	1.31	1.64	1.70
	U1d	3.06	1.70	1.31	0.16	N/M	N/M	N/M	CW	1178.3	1209.4	218.1	1.54	1.10	1.04	1.16	1.64
	U1e	0.43	0.25	0.18	0.00	CCW	CCW	N/M	N/M	231.4	242.2	42.3	0.19	0.62	0.50	0.80	1.17
UV	U1a-V1a	23.77	12.80	10.39	0.69	N/M	N/M	CW	CW	4577.6	4589.4	836.1	13.27	1.14	1.00	1.32	1.41
	U2a-V2a	19.36	9.92	9.41	0.84	N/M	N/M	CW	CW	2666.0	2435.4	537.8	8.83	1.22	1.05	1.42	1.37
	U3a-V3a	15.23	7.00	7.63	0.69	CCW	CCW	N/M	CCW	1023.1	874.2	221.3	3.29	0.78	0.65	0.93	0.62

Supplementary information

Click here to download Supplementary material for on-line publication only: Supplementary information.docx